PUFFERFISH: COMMUNICATION-EFFICIENT MODELS AT NO EXTRA COST

Hongyi Wang [1] **Saurabh Agarwal** [1] **Dimitris Papailiopoulos** [2]

ABSTRACT

To mitigate communication overheads in distributed model training, several studies propose the use of compressed stochastic gradients, usually achieved by sparsification or quantization. Such techniques achieve high compression ratios, but in many cases incur either significant computational overheads or some accuracy loss. In this work, we present PUFFERFISH, a communication and computation efficient distributed training framework that incorporates the gradient compression into the model training process via training low-rank, pre-factorized deep networks. PUFFERFISH not only reduces communication, but also completely bypasses any computation overheads related to compression, and achieves the same accuracy as state-of-the-art, off-the-shelf deep models. PUFFERFISH can be directly integrated into current deep learning frameworks with minimum implementation modification. Our extensive experiments over real distributed setups, across a variety of large-scale machine learning tasks, indicate that PUFFERFISH achieves up to $1.64\times$ end-to-end speedup over the latest distributed training API in PyTorch without accuracy loss. Compared to the *Lottery Ticket Hypothesis* models, PUFFERFISH leads to equally accurate, small-parameter models while avoiding the burden of "winning the lottery". PUFFERFISH also leads to more accurate and smaller models than SOTA structured model pruning methods.

1 INTRODUCTION

Distributed model training plays a key role in the success of modern machine learning systems. Data parallel training, a popular variant of distributed training, has demonstrated massive speedups in real-world machine learning applications and systems (Li et al., 2014; Dean et al., 2012; Chen et al., 2016a). Several machine learning frameworks such as TensorFlow (Abadi et al., 2016) and PyTorch (Paszke et al., 2019) come with distributed implementations of popular training algorithms, such as mini-batch SGD. However, the empirical speed-ups offered by distributed training, often fall short of a best-case linear scaling. It is now widely acknowledged that communication overheads are one of the key sources of this saturation phenomenon (Dean et al., 2012; Seide et al., 2014; Strom, 2015; Qi et al., 2017; Grubic et al., 2018).

Communication bottlenecks are attributed to frequent gradient updates, transmitted across compute nodes. As the number of parameters in state-of-the-art (SOTA) deep models scales to hundreds of billions, the size of communicated gradients scales proportionally (He et al., 2016; Huang et al., 2017; Devlin et al., 2018; 2019; Brown et al., 2020). To reduce the cost of communicating model updates, recent studies propose compressed versions of the computed gradients. A large number of recent studies revisited the idea of low-precision training as a means to reduce communication (Seide et al., 2014; De Sa et al., 2015; Alistarh et al., 2017; Zhou et al., 2016; Wen et al., 2017; Zhang et al., 2017; De Sa et al., 2017; 2018; Bernstein et al., 2018a; Konečnỳ et al., 2016). Other approaches for low-communication training focus on sparsification of gradients, either by thresholding small entries or by random sampling (Strom, 2015; Mania et al., 2015; Suresh et al., 2016; Leblond et al., 2016; Aji & Heafield, 2017; Konečnỳ & Richtárik, 2016; Lin et al., 2017; Chen et al., 2017; Renggli et al., 2018; Tsuzuku et al., 2018; Wang et al., 2018; Vogels et al., 2019).

However, the proposed communication-efficient training techniques via gradient compression usually suffer from some of the following drawbacks: (i) The computation cost for gradient compression (*e.g.*, sparsification or quantization) can be high. For instance, ATOMO (Wang et al., 2018) requires to compute gradient factorizations using SVD for every single batch, which can be computationally expensive for large-scale models. (ii) Existing gradient compression methods either do not fully utilize the full gradients (Alistarh et al., 2017; Wen et al., 2017; Bernstein et al., 2018a; Wang et al., 2018) or require additional memory. For example, the "*error feedback*" scheme (Seide et al., 2014; Stich et al., 2018; Karimireddy et al., 2019) utilizes stale gradients aggregated in memory for future iterations, but requires storing additional information pro-

[1]Department of Computer Sciences, University of Wisconsin-Madison, [2]Department of Electrical and Computer Engineering, University of Wisconsin-Madison. Correspondence to: Hongyi Wang <hongyiwang@cs.wisc.edu>.

Proceedings of the 4^{th} MLSys Conference, San Jose, CA, USA, 2021.

portional to the model size. (iii) Significant implementation efforts are required to incorporate an existing gradient compression technique within high-efficiency distributed training APIs in current deep learning frameworks *e.g.*, `DistributedDataParallel` (DDP) in PyTorch.

Due to the above shortcomings of current communication-efficient techniques, it is of interest to explore the feasibility of incorporating elements of the gradient compression step into the model architecture itself. If this is feasible, then communication efficiency can be attained at no extra cost. In this work, we take a first step towards bypassing the gradient compression step via training low-rank, pre-factorized deep network, starting from full-rank counterparts. We observe that training low-rank models from scratch incurs non-trivial accuracy loss. To mitigate that loss, instead of starting from a low-rank network, we initialize at a full-rank counterpart. We train for a small fraction, *e.g.*, 10% of total number epochs, with the full-rank network, and then convert to a low-rank counterpart. To obtain such a low-rank model we apply SVD on each of the layers. After the SVD step, we use the remaining 90% of the training epochs to fine-tune this low-rank model. The proposed method bares similarities to the "*Lottery Ticket Hypothesis*" (LTH) (Frankle & Carbin, 2018), in that we find "winning tickets" within full-rank/dense models, but without the additional burden of "winning the lottery". Winning tickets seem to be in abundance once we seek models that are sparse in their spectral domain.

Our contributions. In this work, we propose PUFFERFISH, a computation and communication efficient distributed training framework. PUFFERFISH takes any deep neural network architecture and finds a pre-factorized low-rank representation. PUFFERFISH then trains the pre-factorized low-rank network to achieve both computation and communication efficiency, instead of explicitly compressing gradients. PUFFERFISH supports several types of architectures including fully connected (FC), convolutional neural nets (CNNs), LSTMs, and Transformer networks (Vaswani et al., 2017). As PUFFERFISH manipulates the model architectures instead of their gradients, it is directly compatible with all SOTA distributed training frameworks, *e.g.*, PyTorch DDP and BytePS (Jiang et al., 2020).

We further observe that direct training of those pre-factorized low-rank deep networks leads to non-trivial accuracy loss, especially for large-scale machine learning tasks, *e.g.*, ImageNet (Deng et al., 2009). We develop two techniques for mitigating this accuracy loss: (i) a *hybrid architecture* and (ii) *vanilla warm-up training*. The effectiveness of these two techniques is justified via extensive experiments.

We provide experimental results over real distributed systems and large-scale vision and language processing tasks.

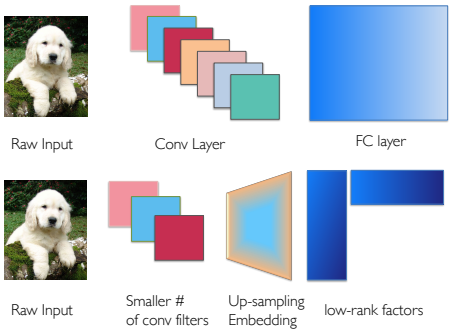

Figure 1. We propose to replace fully connected layers represented by a matrix W, by a set of trainable factors UV^T, and represent each of the N convolutional filters of each conv layer as a linear combination of $\frac{N}{R}$ filters. This latter operation can be achieved by using fewer filters per layer, and then applying a trainable up-sampling embedding to the output channels.

We compare PUFFERFISH against a wide range of SOTA baselines: (i) communication-efficient distributed training methods *e.g.*, POWERSGD (Vogels et al., 2019) and SIGNUM (Bernstein et al., 2018a); (ii) structured pruning methods, *e.g.*, the *Early Bird Ticket* (EB Train) (You et al., 2019); and model sparsification method, *e.g.*, the iterative pruning algorithm in LTH (Frankle & Carbin, 2018). Our experimental results indicate that PUFFERFISH achieves better model training efficiency compared to POWERSGD, SIGNUM, and LTH models. PUFFERFISH also leads to smaller and more accurate model compared to EB Train. We further show that the performance of PUFFERFISH remains stable under *mixed-precision training*.

Related work. PUFFERFISH is closely related to the work on communication-efficient distributed training methods. To reduce the communication cost in distributed training, the related literature has developed several methods for gradient compression. Some of the methods use quantization over the gradient elements (Seide et al., 2014; Alistarh et al., 2017; Wen et al., 2017; Lin et al., 2017; Luo et al., 2017; Bernstein et al., 2018a; Tang et al., 2019; Wu et al., 2018). Other methods study sparsifying the gradients in the element-wise or spectral domains (Lin et al., 2017; Wang et al., 2018; Stich et al., 2018; Vogels et al., 2019). It has also been widely observed that adopting the "*error feedback*" scheme is generally helpful for gradient compression methods to achieve better final model accuracy (Stich et al., 2018; Wu et al., 2018; Karimireddy et al., 2019; Vogels et al., 2019). Compared to the previously proposed gradient compression methods, PUFFERFISH merges the gradient compression into model training, thus achieves communication-efficiency at no extra cost.

PUFFERFISH is also closely related to model compression. Partially initialized by *deep compression* (Han et al., 2015), a lot of research proposes to remove the redundant weights in the trained neural networks. The trained neural networks

can be compressed via model weight pruning (Li et al., 2016; Wen et al., 2016; Hu et al., 2016; Zhu & Gupta, 2017; He et al., 2017; Yang et al., 2017; Liu et al., 2018; Yu et al., 2018b;a), quantization (Rastegari et al., 2016; Zhu et al., 2016; Hubara et al., 2016; Wu et al., 2016; Hubara et al., 2017; Zhou et al., 2017), and low-rank factorization (Xue et al., 2013; Sainath et al., 2013; Jaderberg et al., 2014; Wiesler et al., 2014; Konečnỳ et al., 2016). Different from the model compression methods, PUFFERFISH proposes to train the factorized networks, which achieves better overall training time, rather than compressing the model after fully training it.

Finally, our work is also related to efficient network architecture design, where the network layers are re-designed to be smaller, more compact, and more efficient (Iandola et al., 2016; Chen et al., 2016b; Zhang et al., 2018; Tan & Le, 2019; Howard et al., 2017; Chollet, 2017; Lan et al., 2019; Touvron et al., 2020; Waleffe & Rekatsinas, 2020). The most related low-rank efficient training framework to PUFFERFISH is the one proposed in (Ioannou et al., 2015), where a pre-factorized network is trained from scratch. However, we demonstrate that training the factorized network from scratch leads to non-trivial accuracy loss. In PUFFERFISH, we propose to warm-up the low-rank model via factorizing a partially trained full-rank model. Our extensive experiments indicate that PUFFERFISH achieves significantly higher accuracy compared to training the factorized network from scratch. Moreover, (Ioannou et al., 2015) only studies low-rank factorizations for convolutional layers, whereas PUFFERFISH supports FC, CNN, LSTM, and Transformer layers.

2 PUFFERFISH: EFFECTIVE DEEP FACTORIZED NETWORK TRAINING

In the following subsections, we discuss how model factorization is implemented for different model architectures.

2.1 Low-rank factorization for FC layers

For simplicity, we discuss a 2-layer FC network that can be represented as $h(x) = \sigma(W_1\sigma(W_2x))$ where $W_l, \forall l \in \{1, 2\}$ are weight matrices, $\sigma(\cdot)$ is an arbitrary activation function, and x is the input data point. We propose to pre-factorize the matrices W_l into $U_l V_l^T$ where the factors are of significantly smaller dimensions while also reducing the computational complexity of the full-rank FC layer.

2.2 Low-rank factorization for convolution layers

Basics on convolution layers. The above low-rank factorization strategy extends to convolutional layers (see Fig. 1 for a sketch). In a convolution layer, a c_{in}-channel input image of size $H \times W$ pixels is convolved with c_{out} filters of size $c_{\text{in}} \times k \times k$ to create a c_{out}-channel output feature map. Therefore, the computational complexity for the convolution of the filter with a c_{in}-channel input image is $\mathcal{O}(c_{\text{in}}c_{\text{out}}k^2HW)$. In what follows, we describe schemes for modifying the architecture of the convolution layers via low-rank factorization to reduce computational complexity and the number of parameters. The idea is to replace vanilla (full-rank) convolution layers with factorized versions. These factorized filters amount to the same number of convolution filters, but are constructed through linear combinations of a sparse, *i.e.*, low-rank filter basis.

Factorizing a convolution layer. For a convolution layer with dimension $W \in \mathbb{R}^{c_{\text{in}} \times c_{\text{out}} \times k \times k}$ where c_{in} and c_{out} are the number of input and output channels and k is the size of the convolution filters, *e.g.*, $k = 3$ or 5. Instead of factorizing the 4D weight of a convolution layer directly, we consider factorizing the unrolled 2D matrix. Unrolling the 4D tensor W leads to a 2D matrix with shape $W_{\text{unrolled}} \in \mathbb{R}^{c_{\text{in}}k^2 \times c_{\text{out}}}$ where each column represents the weight of a vectorized convolution filter. The rank of the unrolled matrix is determined by $\min\{c_{\text{in}}k^2, c_{\text{out}}\}$. Factorizing the unrolled matrix returns $U \in \mathbb{R}^{c_{\text{in}}k^2 \times r}$, $V^\top \in \mathbb{R}^{r \times c_{\text{out}}}$, *i.e.*, $W_{\text{unrolled}} \approx UV^\top$. Reshaping the factorized $U, V^\top$ matrices back to 4D filters leads to $U \in \mathbb{R}^{c_{\text{in}} \times r \times k \times k}, V^\top \in \mathbb{R}^{r \times c_{\text{out}}}$. Therefore, factorizing a convolution layer returns a thinner convolution layer U with width r, *i.e.*, the number of convolution filters, and a linear projection layer $V^\top$. In other words, the full-rank original convolution filter bank is approximated by a linear combination of r basis filters. The $V^\top$s can also be represented by a 1×1 convolution layer, *e.g.*, $V_l^\top \in \mathbb{R}^{r \times c_{\text{out}} \times 1 \times 1}$, which is more natural for computer vision tasks as it operates directly on the spatial domain (Lin et al., 2013). In PUFFERFISH, we use the 1×1 convolution for all $V_l^\top$ layers in the considered CNNs. One can also use tensor decomposition, *e.g.*, the Tucker decomposition to directly factorize the 4D tensor weights (Tucker, 1966). In this work, for simplicity, we do not consider tensor decompositions.

2.3 Low-rank factorization for LSTM layers

LSTMs have been proposed as a means to mitigate the "vanishing gradient" issue of traditional RNNs (Hochreiter & Schmidhuber, 1997). The forward pass of an LSTM is as follows

$$
\begin{aligned}
i_t &= \sigma(W_{ii}x_t + b_{ii} + W_{hi}h_{t-1} + b_{hi}) \\
f_t &= \sigma(W_{if}x_t + b_{if} + W_{hf}h_{t-1} + b_{hf}) \\
g_t &= \tanh(W_{ig}x_t + b_{ig} + W_{hg}h_{t-1} + b_{hg}) \\
o_t &= \sigma(W_{io}x_t + b_{io} + W_{ho}h_{t-1} + b_{ho}) \\
c_t &= f_t \odot c_{t-1} + i_t \odot g_t \\
h_t &= o_t \odot \tanh(c_t).
\end{aligned} \tag{1}
$$

h_t, c_t, x_t represent the hidden state, cell state, and input at time t respectively. h_{t-1} is the hidden state of the layer at time $t-1$. i_t, f_t, g_t, o_t are the input, forget, cell, and output gates, respectively. $\sigma(\cdot)$ and $\odot$ denote the sigmoid activation function and the Hadamard product, respectively. The trainable weights are the matrices $W_{i\cdot} \in \mathbb{R}^{h \times d}, W_{h\cdot} \in \mathbb{R}^{h \times h}$, where d and h are the embedding and hidden dimensions. Thus, similarly to the low-rank FC layer factorization, the factorized LSTM layer is represented by

$$
\begin{aligned}
i_t &= \sigma(U_{ii}V_{ii}^\top x_t + b_{ii} + U_{hi}V_{hi}^\top h_{t-1} + b_{hi}) \\
f_t &= \sigma(U_{if}V_{if}^\top x_t + b_{if} + U_{hf}V_{hf}^\top h_{t-1} + b_{hf}) \\
g_t &= \tanh(U_{ig}V_{ig}^\top x_t + b_{ig} + U_{hg}V_{hg}^\top h_{t-1} + b_{hg}) \\
o_t &= \sigma(U_{io}V_{io}^\top x_t + b_{io} + U_{ho}V_{ho}^\top h_{t-1} + b_{ho}) \\
c_t &= f_t \odot c_{t-1} + i_t \odot g_t \\
h_t &= o_t \odot \tanh(c_t).
\end{aligned} \tag{2}
$$

2.4 Low-rank network factorization for Transformer

A Transformer layer consists of a stack of encoders and decoders (Vaswani et al., 2017). Both encoder and decoder contain three main building blocks, *i.e.*, the *multi-head attention* layer, *position-wise feed-forward networks* (FFN), and *positional encoding*. A p-head attention layer learns p independent attention mechanisms on the input key (K), value (V), and queries (Q) of each input token:

$$
\begin{aligned}
\text{MultiHead}(Q, K, V) &= \text{Concat}(\text{head}_1, \cdots, \text{head}_p)W^O \\
\text{where head}_i &= \text{Attention}(QW_i^Q, KW_i^K, VW_i^V).
\end{aligned}
$$

In the above, $W_i^Q, W_i^K, W_i^V, i \in \{1, \cdots, p\}$ are trainable weight matrices. The particular attention, referred to as "scaled dot-product attention", is used in Transformers, *i.e.*, $\text{Attention}(\tilde{Q}, \tilde{K}, \tilde{V}) = \text{softmax}\left(\frac{\tilde{Q}\tilde{K}^\top}{\sqrt{d}}\right)\tilde{V}$ where $\tilde{Q} = QW_i^Q, \tilde{K} = KW_i^K, \tilde{V} = VW_i^V$. W^O projects the output of the multi-head attention layer to match the embedding dimension. Following (Vaswani et al., 2017), we assume the projected key, value, and query are embedded to pd dimensions, and are projected to d dimensions in the attention layer. In Transformer, a sequence of N input tokens are usually batched before passing to the model where each input token is embedded to a pd dimensional vector. Thus, dimensions of the inputs are $Q, K, V \in \mathbb{R}^{N \times pd}$. The learnable weight matrices are $W_i^Q, W_i^K, W_i^V \in \mathbb{R}^{pd \times d}, W^O \in \mathbb{R}^{pd \times pd}$. The FFN in Transformer consists of two learnable FC layers: $\text{FFN}(x) = \max(0, xW_1 + b_1)W_2 + b_2$ where $W_1 \in \mathbb{R}^{pd \times 4pd}, W_2 \in \mathbb{R}^{4pd \times pd}$ (the relationships between the notations in our paper and the original Transformer paper (Vaswani et al., 2017) are $pd = d_{\text{model}}, d = d_k = d_v$, and $d_{ff} = 4pd$).

In PUFFERFISH, we factorize all learnable weight matrices in the multi-head attention and the FFN layers. We leave the positional encoding as is, since there are no trainable weights. For the bias term of each layer and the "*Layer Normalization*" weights, we use the vanilla weights directly, as they are represented by vectors.

Table 1. The number of parameters and computational complexities for full-rank and low-rank FC, convolution, LSTM, and the Transformer layers where m, n are the dimensions of the FC layer and $c_{\text{in}}, c_{\text{out}}, k$ are the input, output dimensions, and kernel size respectively. h, d denote the hidden and embedding dimensions in the LSTM layer. N, p, d denote the sequence length, number of heads, and embedding dimensions in the Transformer. r denotes the rank of the factorized low-rank layer we assume to use.

Networks	# Params.	Computational Complexity
Vanilla FC	$m \times n$	$\mathcal{O}(mn)$
Factorized FC	$r(m+n)$	$\mathcal{O}(r(m+n))$
Vanilla Conv.	$c_{\text{in}} \times c_{\text{out}} \times k^2$	$\mathcal{O}(c_{\text{in}}c_{\text{out}}k^2HW)$
Factorized Conv.	$c_{\text{in}}rk^2 + rc_{\text{out}}$	$\mathcal{O}(rc_{\text{in}}k^2HW + rHWc_{\text{out}})$
Vanilla LSTM	$4(dh+h^2)$	$\mathcal{O}(dh+h^2)$
Factorized LSTM	$4dr + 12hr$	$\mathcal{O}(dr+hr)$
Vanilla Attention	$4p^2d^2$	$\mathcal{O}(Np^2d^2 + N^2d)$
Factorized Attention	$(3p+5)prd$	$\mathcal{O}(rpdN + N^2d)$
Vanilla FFN	$8p^2d^2$	$\mathcal{O}(p^2d^2N)$
Factorized FFN	$10pdr$	$\mathcal{O}(rpdN)$

2.5 Computational complexity and model size

A low-rank factorized network enjoys a smaller number of parameters and lower computational complexity. Thus, both the computation and communication efficiencies are improved, as the amount of communication is proportional to the number of parameters. We summarize the computational complexity and the number of parameters in the vanilla and low-rank FC, convolution, LSTM, and the Transformer layers in Table 1. We assume the FC layer has shape $W_{FC} \in \mathbb{R}^{m \times n}$, the convolution layer has shape $W_{\text{Conv}} \in \mathbb{R}^{c_{\text{in}} \times c_{\text{out}} \times k \times k}$, the LSTM layer has shape $W_i \in \mathbb{R}^{4h \times d}; W_h \in \mathbb{R}^{4h \times h}$ (where W_i and W_h is the concatenated input-hidden and hidden-hidden weight matrices), and the shapes of the model weights in the encoder of a Transformer follow the discussion in Section 2.4. For the number of parameters, we do not count the bias terms. For Transformers, we show the computational complexity of a single encoder block. We assume the low-rank layers have rank r. As the computation across the p heads can be done in parallel, we report the computational complexity of a single attention head. Note that for the LSTM layer, our complexity analysis assumes the low-rank layer uses the same rank for the input-hidden weights $W_{i\cdot}$ and the hidden-hidden weights $W_{h\cdot}$. Similarly, for the Transformer layer, we assume the low-rank layer uses the same rank r for all W_i^Q, W_i^K, W_i^V, W^O. Further details can be found in the Appendix.

3 STRATEGIES FOR MITIGATING ACCURACY LOSS

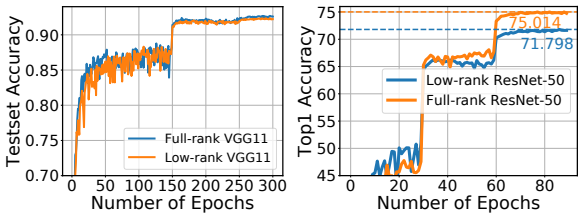

(a) VGG-11 on CIFAR-10 (b) ResNet-50 on ImageNet

Figure 2. Model convergence comparisons between vanilla models and PUFFERFISH factorized models: (a) low-rank VGG-11 over the CIFAR-10 dataset; (b) ResNet-50 over the ImageNet dataset. For the low-rank networks, all layers except for the first convolution and the very last FC layer are factorized with a fixed rank ratio at 0.25.

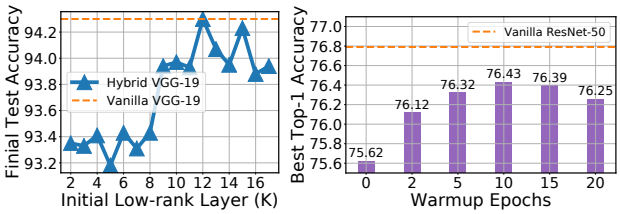

(a) Hybrid network (b) Vanilla warm-up training

Figure 3. The effect of the test accuracy loss mitigation methods in PUFFERFISH: (a) **Hybrid network**: The final test accuracy of the hybrid VGG-19 architectures with various initial low-rank layer indices (K) over the CIFAR-10 dataset. (b) **Vanilla warm-up training**: The final top-1 accuracy of the hybrid-ResNet-50 architecture trained on the ImageNet dataset under the different number of vanilla warm-up epochs: $\{2, 5, 10, 15, 20\}$.

In this section, we showcase that training low-rank models from scratch leads to an accuracy loss. Interestingly, this loss can be mitigated by balancing the degree of factorization across layers, and by using a short full-rank warm-up training phase used to initialize the factorized model.

We conduct an experimental study on a version of PUFFERFISH where every layer of the network is factorized except for the first convolution layer and the last FC layer. On a relatively small task, *e.g.*, VGG-11 on CIFAR-10, we observe that PUFFERFISH only leads to $\sim 0.4\%$ accuracy loss (as shown in Figure 3) compared to the vanilla VGG-19-BN. However, for ResNet-50 on the ImageNet dataset, a $\sim 3\%$ top-1 accuracy loss of PUFFERFISH is observed. To mitigate the accuracy loss of the factorized networks over the large-scale ML tasks, we propose two methods, *i.e.*, (i) *hybrid network architecture* and (ii) *vanilla warm-up training*. We then discuss each method separately.

Hybrid network architecture. In PUFFERFISH, the low-rank factorization aims at approximating the original network weights, *i.e.*, $W_l \approx U_l V_l^\top$ for layer l, which inevitably introduces approximation error. Since the approximation error in the early layers can be accumulated and propagated to the later layers, a natural strategy to mitigate the model accuracy loss is to only factorize the later layers. Moreover, for most of CNNs, the number of parameters in later layers dominates the entire network size. Thus, factorizing the later layers does not sacrifice the degree of model compression we can achieve. Specifically, for an L layer network $\{W_1, W_2, \cdots, W_L\}$, factorizing every layer leads to $\{U_1, V_1^\top, U_2, V_2^\top, \cdots, U_L, V_L^\top\}$. In the hybrid network architecture, the first $K-1$ layers are not factorized, *i.e.*, $\{W_1, W_2, \cdots, W_{K-1}, U_K, V_K^\top, \cdots, U_L, V_L^\top\}$ where we define K as the index of the first low-rank layer in a hybrid architecture. We treat K as a hyper-parameter, which balances the model compression ratio and the final model accuracy. In our experiments, we tune K for all models. The effectiveness of the hybrid network architecture is shown in Figure 3(a), from which we observe that the hybrid VGG-19 with $K = 9$ mitigates $\sim 0.6\%$ test accuracy loss.

Algorithm 1 PUFFERFISH Training Procedure

Input : Randomly initialized weights of vanilla N-layer architectures $\{W_1, W_2, \ldots, W_L\}$, and the associated weights of hybrid N-layer architecture $\{W_1, W_2, \ldots, W_{K-1}, U_K, V_K^\top, \ldots, U_L, V_L^\top\}$, the entire training epochs E, the vanilla warm-up training epochs E_{wu}, and learning rate schedule $\{\eta_t\}_{t=1}^{E}$

Output : Trained hybrid L-layer architecture weights $\{\hat{W}_1, \hat{W}_2, \ldots, \hat{W}_{K-1}, \hat{U}_K, \hat{V}_K^\top, \ldots, \hat{U}_L, \hat{V}_L^\top\}$

for $t \in \{1, \ldots, E_{wu}\}$ **do**
  Train $\{W_1, W_2, \ldots, W_L\}$ with learning rate schedule $\{\eta_t\}_{t=1}^{E_{wu}}$; `// vanilla warm-up training`
end
for $l \in \{1, \ldots, L\}$ **do**
  if $l < K$ **then**
    copy the partially trained W_l weight to the hybrid network;
  else
    $\tilde{U}_l \Sigma_l \tilde{V}_l^\top = \text{SVD}(W_l)$; `// Decomposing the vanilla warm-up trained weights`
    $U_l = \tilde{U}_l \Sigma_l^{\frac{1}{2}}, V_l^\top = \Sigma^{\frac{1}{2}} \tilde{V}_l^\top$
  end
end
for $t \in \{E_{wu}+1, \ldots, E\}$ **do**
  Train the hybrid network weights, *i.e.*, $\{W_1, W_2, \ldots, W_{K-1}, U_K, V_K^\top, \ldots, U_L, V_L^\top\}$ with learning rate schedule $\{\eta_t\}_{t=E_{wu}}^{E}$; `// consecutive low rank training`
end

Vanilla warm-up training. It has been widely observed that epochs early in training are critical for the final model accuracy (Jastrzebski et al., 2020; Keskar et al., 2016; Achille et al., 2018; Leclerc & Madry, 2020; Agarwal et al., 2020). For instance, sparsifying gradients in early training phases can hurt the final model accuracy (Lin et al., 2017). Similarly, factorizing the vanilla model weights in the very beginning of the training procedure can also lead to accuracy

loss, which may be impossible to mitigate in later training epochs. It has also been shown that good initialization strategies play a significant role in the final model accuracy (Zhou et al., 2020).

In this work, to mitigate the accuracy loss, we propose to use the partially trained vanilla, full-rank model weights to initialize the low-rank factorized network. We refer to this as "*vanilla warm-up training*". We train the vanilla model for a few epochs (E_{wu}) first. Then, we conduct truncated matrix factorization (via truncated SVD) over the partially trained model weights to initialize the low-rank factors. For instance, given a partially trained FC layer $W^{(l)}$, we deploy SVD on it such that we get $\tilde{U}\Sigma\tilde{V}^\top$. After that the U and $V^\top$ weights we introduced in the previous sections can be found by $U = \tilde{U}\Sigma^{\frac{1}{2}}, V^\top = \Sigma^{\frac{1}{2}}\tilde{V}^\top$. For convolution layer $W \in \mathbb{R}^{c_{\text{in}} \times c_{\text{out}} \times k \times k}$, we conduct SVD over the unrolled 2D matrix $W_{\text{unrolled}} \in \mathbb{R}^{c_{\text{in}}k^2 \times c_{\text{out}}}$, which leads to $U \in \mathbb{R}^{c_{\text{in}}k^2 \times r}, V^\top \in \mathbb{R}^{r \times c_{\text{out}}}$ where reshaping U, V back to 4D leads to the desired initial weights for the low-rank layer, *i.e.*, $U \in \mathbb{R}^{r \times c_{\text{out}} \times k \times k}, V^\top \in \mathbb{R}^{r \times c_{\text{out}} \times 1 \times 1}$. For the Batch Normalization layers (BNs) (Ioffe & Szegedy, 2015) we simply extract the weight vectors and the collected running statistics, *e.g.*, the *running mean and variance*, for initializing the low-rank training. We also directly take the bias vector of the last FC layer. PUFFERFISH then finishes the remaining training epochs over the factorized hybrid network initialized with vanilla warm-up training.

Figure 3(b) provides an experimental justification on the effectiveness of vanilla warm-up training where we study a hybrid ResNet-50 trained on the ImageNet dataset. The results indicate that vanilla warm-up training helps to improve the accuracy of the factorized model. Moreover, a carefully tuned warm-up period of $\hat{E}_{wu}$ also plays an important role in the final model accuracy. Though SVD is computationally heavy, PUFFERFISH only requires to conduct the SVD **once** throughout the entire training. We benchmark the SVD cost for all experimented models, which indicate the SVD runtime is comparatively small, *e.g.*, on average, it only costs 2.29 seconds for ResNet-50. A complete study on the SVD factorization overheads can be found in the Appendix.

Last FC layer. The very last FC layer in a neural network can be viewed as a linear classifier over the features extracted by the previous layers. In general, its rank is equal to the number of classes in predictve task at hand. Factorizing it below the number of classes, will increase linear dependencies, and may further increase the approximation error. Thus, PUFFERFISH does not factorize it.

Putting all the techniques we discussed in this section together, the training procedure of PUFFERFISH is summarized in Algorithm 1.

4 EXPERIMENTS

We conduct extensive experiments to study the effectiveness and scalability of PUFFERFISH over various computer vision and natural language processing tasks, across real distributed environments. We also compare PUFFERFISH against a wide range of baselines including: (i) POWERSGD, a low-rank based, gradient compression method that achieves high compression ratios (Vogels et al., 2019); (ii) SIGNUM a gradient compression method that only communicates the sign of the local momentum (Bernstein et al., 2018a;b); (iii) The "early bird" structured pruning method *EB Train* (You et al., 2019); and (iv) The LTH sparsification method (referred to as LTH for simplicity) (Frankle & Carbin, 2018).

Our experimental results indicate that PUFFERFISH allows to train a model that is up to $3.35\times$ smaller than other methods, with only marginal accuracy loss. Compared to POWERSGD, SIGNUM, and vanilla SGD, PUFFERFISH achieves $1.22\times$, $1.52\times$, and $1.74\times$ end-to-end speedups respectively for ResNet-18 trained on CIFAR-10 while reaching to the same accuracy as vanilla SGD. PUFFERFISH leads to a model with $1.3M$ fewer parameters while reaching 1.76% higher top-1 test accuracy than EB Train on the ImageNet dataset. Compared to LTH, PUFFERFISH leads to $5.67\times$ end-to-end speedup for achieving the same model compression ratio for VGG-19 on CIFAR-10. We also demonstrate that the performance of PUFFERFISH is stable under the "mixed-precision training" implemented by PyTorch AMP. Our code is publicly available for reproducing our results[1].

4.1 Experimental setup and implementation details

Setup. PUFFERFISH is implemented in PyTorch (Paszke et al., 2019). We experiment using two implementations. The first implementation we consider is a data-parallel model training API, *i.e.*, DDP in PyTorch. However, as the gradient computation and communication are overlapped in DDP[2], it is challenging to conduct a breakdown runtime analysis in DDP. We thus also come up with a prototype `allreduce`-based distributed implementation that decouples the computation and communication to benchmark the breakdown runtime of PUFFERFISH and other baselines. Our prototype distributed implementation is based on `allreduce` in PyTorch and the NCCL backend. All our experiments are deployed on a distributed cluster consisting of up to 16 `p3.2xlarge` (Tesla V100 GPU equipped) instances on Amazon EC2.

Models and Datasets. The datasets considered in our experiments are CIFAR-10 (Krizhevsky et al., 2009), Ima-

[1] https://github.com/hwang595/Pufferfish

[2] the computed gradients are buffered and communicated immediately when hitting a certain buffer size, *e.g.*, 25MB.

geNet (ILSVRC2012) (Deng et al., 2009), the WikiText-2 datasets (Merity et al., 2016), and the WMT 2016 German-English translation task data (Elliott et al., 2016). For the image classification tasks on CIFAR-10, we considered VGG-19-BN (which we refer to as VGG-19) (Simonyan & Zisserman, 2014) and ResNet-18 (He et al., 2016). For ImageNet, we run experiments with ResNet-50 and WideResNet-50-2 (Zagoruyko & Komodakis, 2016). For the WikiText-2 dataset, we considered a 2-layer stacked LSTM model. For the language translation task, we consider a 6-layer Transformer architecture (Vaswani et al., 2017). More details about the datasets and models can be found in the Appendix.

Implementation details and optimizations. In our prototype distributed implementation, the `allreduce` operation starts right after all compute nodes finish computing the gradient. An important implementation-level optimization we conduct is that we pack all gradient tensors into one flat buffer, and only call the `allreduce` operation **once** per iteration. The motivation for such an optimization is that PUFFERFISH factorizes the full-rank layer W_l to two smaller layers, *i.e.*, $U_l, V_l^\top$. Though the communication cost of the `allreduce` on each smaller layer is reduced, the total number of `allreduce` calls is doubled (typically an `allreduce` is required per layer to synchronize the gradients across the distributed cluster). According to the run-time cost model of the ring-allreduce (Thakur et al., 2005), each `allreduce` call introduces a network latency proportional to the product of the number of compute nodes and average network latency. This is not a negligible cost. Our optimization strategy aims at minimizing the additional latency overhead and leads to good performance improvement based on our tests. For a fair comparison, we conduct the same communication optimization for all considered baselines.

Table 2. The results (averaged across 3 independent trials with different random seeds) of PUFFERFISH and the vanilla 2-layer stacked LSTMs trained over the WikiText-2 dataset (since the embedding layer is just a look up table, we do not count it when calculating the MACs).

Model archs.	Vanilla LSTM	PUFFERFISH LSTM
# Params.	$85,962,278$	$67,962,278$
Train Ppl.	52.87 ± 2.43	62.2 ± 0.74
Val Ppl.	92.49 ± 0.41	93.62 ± 0.36
Test Ppl.	88.16 ± 0.39	88.72 ± 0.24
MACs	18M	9M

Hyper-parameters for PUFFERFISH. For all considered model architectures, we use a global rank ratio of 0.25, *e.g.*, for a convolution layer with an initial rank of 64, PUFFERFISH sets $r = 64 \times 0.25 = 16$. For the LSTM on WikiText-2 experiment, we only factorize the LSTM layers and leave the tied embedding layer as is. Allocating the optimal rank for each layer can lead to better final model accuracy and smaller model sizes as discussed in (Idelbayev & Carreira-Perpinán, 2020). However, the search space for the rank allocation problem is large. One potential way to solve that problem is to borrow ideas from the literature of neural architectural search (NAS), which we leave as future work. We tune the initial low-rank layer index, *i.e.*, K and the vanilla warm-up training period to balance the hybrid model size and the final model accuracy. More details of the hyper-parameters of PUFFERFISH can be found in the Appendix.

Table 3. The results (averaged across 3 independent trials with different random seeds) of PUFFERFISH and vanilla 6-layer Transformers trained over the WMT 2016 German to English Translation Task.

Model archs.	Vanilla Transformer	PUFFERFISH Transformer
# Params.	$48,978,432$	$26,696,192$
Train Ppl .	13.68 ± 0.96	$\mathbf{10.27 \pm 0.65}$
Val. Ppl .	11.88 ± 0.43	$\mathbf{7.34 \pm 0.12}$
Test BLEU	19.05 ± 0.59	$\mathbf{26.87 \pm 0.17}$

Table 4. The results (averaged across 3 independent trials with different random seeds) of PUFFERFISH and vanilla VGG-19 and ResNet-18 trained over the CIFAR-10 dataset. Both full-precision training (FP32) and "mixed-precision training" (AMP) results are reported.

Model Archs.	# Params.	Test Acc. (%)	MACs (G)
Vanilla VGG-19 (FP32)	$20,560,330$	93.91 ± 0.01	0.4
PUFFERFISH VGG-19 (FP32)	$8,370,634$	93.89 ± 0.14	0.29
Vanilla VGG-19 (AMP)	$20,560,330$	94.12 ± 0.08	N/A
PUFFERFISH VGG-19 (AMP)	$8,370,634$	93.98 ± 0.06	N/A
Vanilla ResNet-18 (FP32)	$11,173,834$	95.09 ± 0.01	0.56
PUFFERFISH ResNet-18 (FP32)	$3,336,138$	94.87 ± 0.21	0.22
Vanilla ResNet-18 (AMP)	$11,173,834$	95.02 ± 0.1	N/A
PUFFERFISH ResNet-18 (AMP)	$3,336,138$	94.70 ± 0.37	N/A

4.2 Results

Parameter reduction and model accuracy. We extensively study the effectiveness of PUFFERFISH, and the comprehensive numerical results are shown in Table 2, 3, 4, and 5. The main observation is that PUFFERFISH effectively reduces the number of parameters while introducing only marginal accuracy loss. In particular, PUFFERFISH ResNet-18 is $3.35\times$ smaller than vanilla ResNet-18 with only 0.22% accuracy loss. Surprisingly, the PUFFERFISH Transformer leads to even better validation perplexity and test BLEU scores than the vanilla Transformer. One potential reason behind that is that factorizing the Transformer introduces some implicit regularization, leading to better generaliza-

Table 5. The results of the vanilla and PUFFERFISH ResNet-50 and WideResNet-50-2 models trained on the ImageNet dataset. For the ResNet-50 results, both full precision training (FP32) and mixed-precision training (AMP) are provided. For the AMP training, MACs are not calculated.

Model Archs.	Number of Parameters	Final Test Acc. (Top-1)	Final Test Acc. (Top-5)	MACs (G)
Vanilla WideResNet-50-2 (FP32)	68, 883, 240	78.09%	94.00%	11.44
PUFFERFISH WideResNet-50-2 (FP32)	40, 047, 400	77.84%	93.88%	9.99
Vanilla ResNet-50 (FP32)	25, 557, 032	76.93%	93.41%	4.12
PUFFERFISH ResNet-50 (FP32)	15, 202, 344	76.43%	93.10%	3.6
Vanilla ResNet-50 (AMP)	25, 557, 032	76.97%	93.35%	N/A
PUFFERFISH ResNet-50 (AMP)	15, 202, 344	76.35%	93.22%	N/A

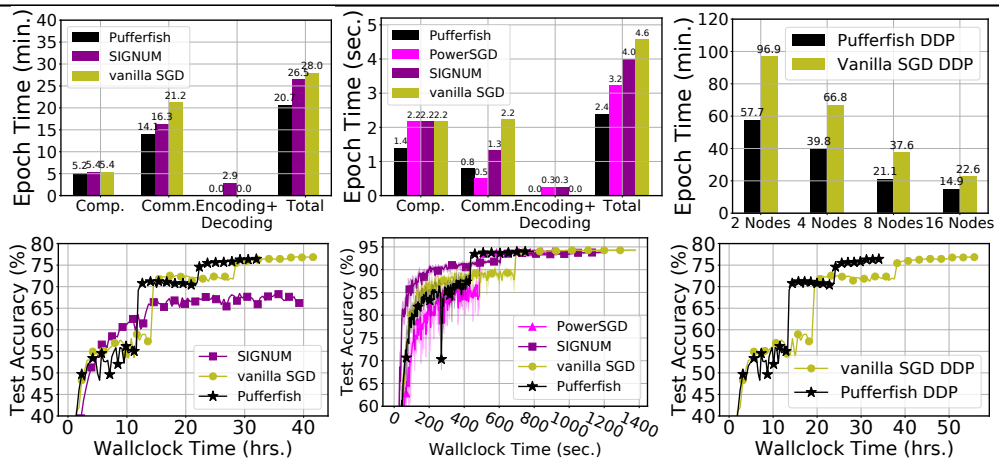

(a) Proto. ResNet-50, ImageNet (b) Proto. ResNet-18, CIFAR-10 (c) DDP ResNet-50, ImageNet

Figure 4. (a) Breakdown per-epoch runtime analysis (top) and end-to-end convergence (bottom) results for vanilla SGD, PUFFERFISH, and SIGNUM over ResNet-50 trained on the ImageNet dataset. Where `Comm.` and `Comp.` stands for computation and communication costs; (b) Breakdown per-epoch runtime analysis (top) and end-to-end convergence (bottom) results for vanilla SGD, PUFFERFISH, SIGNUM, and PowerSGD over ResNet-18 trained on CIFAR-10; (c) The scalability of PUFFERFISH compared to vanilla SGD for ResNet-50 training on ImageNet using PyTorch DDP over the distributed clusters that consist of 2, 4, 8, 16 nodes (top); End-to-end convergence for vanilla SGD and PUFFERFISH with PyTorch DDP under the cluster with 8 nodes (bottom).

Table 6. The runtime mini-benckmark results of PUFFERFISH and vanilla VGG-19 and ResNet-18 networks training on the CIFAR-10 dataset. Experiment running on a single V100 GPU with batch size at 128, results averaged over 10 epochs; under the reproducible cuDNN setup with `cudnn.benckmark` disabled and `cudnn.deterministic` enabled; Speedup calculated based on the averaged runtime.

Model Archs.	Epoch Time (sec.)	Speedup	MACs (G)
Vanilla VGG-19	13.51 ± 0.02	–	0.4
PUFFERFISH VGG-19	$\mathbf{11.02 \pm 0.01}$	$\mathbf{1.23\times}$	**0.29**
Vanilla ResNet-18	18.89 ± 0.07	–	0.56
PUFFERFISH ResNet-18	$\mathbf{12.78 \pm 0.03}$	$\mathbf{1.48\times}$	**0.22**

tion. Apart from the full precision training over FP32, we also conduct mixed-precision experiments over PyTorch AMP on both CIFAR-10 and ImageNet. Our results generally demonstrate that the performance of PUFFERFISH remains stable under mixed-precision training. We measure the computational complexity using "*multiply–accumulate operations*" (MACs) [3]. The MAC results are shown in Table 2, 4, and 5. The computation complexity is estimated by passing a single input through the entire network, *e.g.*, for the CIFAR-10 dataset, we simulate a color image with size $32 \times 32 \times 3$ and pass it to the networks. For the LSTM network, we assume a single input token is with batch size at 1. We only report the MACs of forward pass. PUFFERFISH reduces the MACs of the vanilla model to up to $2.55\times$ over ResNet-18 on CIFAR-10.

Runtime mini-benchmark. It is of interest to investigate the actual speedup of the factorized networks as they are dense and compact. We thus provide mini-benchmark runtime results over VGG-19 and ResNet-18 on the CIFAR-10 dataset. We measure the per-epoch training speed of the factorized networks used in PUFFERFISH and the vanilla networks on a single V100 GPU with batch size at 128. The results are shown in Table 6. We report the results (averaged over 10 epochs) under the reproducibility op-

[3] https://en.wikipedia.org/wiki/Multiply%E2%80%93accumulate_operation

timized cuDNN environment, *i.e.*, `cudnn.benckmark` disabled and `cudnn.deterministic` enabled. The results indicate that the factorized networks enjoy promising runtime speedups, *i.e.*, $1.23\times$ and $1.48\times$ over the vanilla VGG-19 and ResNet-18 respectively. We also study the runtime of the factorized networks under the speed optimized cuDNN setting, *i.e.*, `cudnn.benckmark` enabled and `cudnn.deterministic` disabled, the results can be found in the Appendix.

Computation and communication efficiency. To benchmark the computation and communication costs of PUFFERFISH under a distributed environment, we conduct a per-epoch breakdown runtime analysis and compare it to vailla SGD and SIGNUM on ResNet-50, trained over ImageNet. The experiment is conducted over 16 `p3.2xlarge` EC2 instances. We set the global batch size at 256 (16 per node). We use tuned hyper-parameters for all considered baselines. The result is shown in Figure 4(a) where we observe that the PUFFERFISH ResNet-50 achieves $1.35\times$ and $1.28\times$ per-epoch speedups compared to vanilla SGD and SIGNUM respectively. Note that though SIGNUM achieves high compression ratio, it is not compatible with `allreduce`, thus `allgather` is used instead in our SIGNUM implementation. However, `allgather` is less efficient than `allreduce`, which hurts the communication efficiency of SIGNUM. The effect has also been observed in the previous literature (Vogels et al., 2019). We extend the per-epoch breakdown runtime analysis to ResNet-18 trainining on CIFAR-10 where we compare PUFFERFISH to POWERSGD, SIGNUM, and vanilla SGD. The experiments are conducted over 8 `p3.2xlarge` EC2 instances with the global batch size at 2048 (256 per node). We use a linear learning rate warm-up for 5 epochs from 0.1 to 1.6, which follows the setting in (Vogels et al., 2019; Goyal et al., 2017). For POWERSGD, we set the rank at 2, as it matches the same accuracy compared to vanilla SGD (Vogels et al., 2019). The results are shown in Figure 4(b), from which we observe that PUFFERFISH achieves $1.33\times, 1.67\times, 1.92\times$ per-epoch speedups over POWERSGD, SIGNUM, and vanilla SGD respectively. Note that PUFFERFISH is slower than POWERSGD in the communication stage since POWERSGD massively compresses gradient and is also compatible with `allreduce`. However, PUFFERFISH is faster for gradient computing and bypasses the gradient encoding and decoding steps. Thus, the overall epoch time cost of PUFFERFISH is faster than POWERSGD. Other model training overheads, *e.g.*, data loading and pre-processing, gradient flattening, and etc are not included in the "computation" stage but in the overall per-epoch time.

Since PUFFERFISH only requires to modify the model architectures instead of gradients, it is directly compatible with current data-parallel training APIs, *e.g.*, DDP in PyTorch. Other gradient compression methods achieve high compression ratio, but they are not directly compatible with DDP without significant engineering effort. For PyTorch DDP, we study the speedup of PUFFERFISH over vanilla distributed training, measuring the per-epoch runtime on ResNet-50 and ImageNet over distributed clusters of size $2, 4, 8$, and 16. We fix the per-node batch size at 32 following the setup in (Goyal et al., 2017). The results are shown in Figure 4(c). We observe that PUFFERFISH consistently outperforms vanilla ResNet-50. In particular, on the cluster with 16 nodes, PUFFERFISH achieves $1.52\times$ per epoch speedup.

End-to-end speedup. We study the end-to-end speedup of PUFFERFISH against other baselines under both our prototype implementation and PyTorch DDP. The experimental setups for the end-to-end experiment are identical to our per-epoch breakdown runtime analysis setups. All reported runtimes include the overheads of the SVD factorization and vanilla warm-up training. The ResNet-50 on ImageNet convergence results with our prototype implementation are shown in Figure 4(a). We observe that to finish the entire 90 training epochs, PUFFERFISH attains $1.3\times$ and $1.23\times$ end-to-end speedups compared to vanilla SGD and SIGNUM respectively. The ResNet-18 on CIFAR-10 convergence results are shown in Figure 4(b). For faster vanilla warm-up training in PUFFERFISH, we deploy POWERSGD to compress the gradients. We observe that it is generally better to use a slightly higher rank for POWERSGD in the vanilla warm-up training period of PUFFERFISH. In our experiments, we use POWERSGD with rank 4 to warm up PUFFERFISH. We observe that to finish the entire 300 training epochs, PUFFERFISH attains $1.74\times, 1.52\times, 1.22\times$ end-to-end speedup compared to vanilla SGD, SIGNUM, and POWERSGD respectively. PUFFERFISH reaches to the same accuracy compared to vanilla SGD. Moreover, we extend the end-to-end speedup study under PyTorch DDP where we compare PUFFERFISH with vanilla SGD under 8 EC2 `p3.2xlarge` instances. The global batch size is 256 (32 per node). The results are shown in Figure 4(c) where we observe that to train the model for 90 epochs, PUFFERFISH achieves $1.64\times$ end-to-end speedup compared to vanilla SGD. We do not study the performance of SIGNUM and POWERSGD under DDP since they are not directly compatible with DDP.

Comparison with structured pruning. We compare PUFFERFISH with the EB Train method where structured pruning is conducted over the channel dimensions based on the activation values during the early training phase (You et al., 2019). EB Train finds compact and dense models. The result is shown in Table 7. We observe that compared to EB Train with prune ratio $(pr) = 30\%$, PUFFERFISH returns a model with $1.3M$ fewer parameters while reaching 1.76% higher top-1 test accuracy. The EB Train experimental results are taken directly from the original paper (You et al.,

Table 7. Comparison of Hybrid ResNet-50 model compared to the Early-Bird Ticket structure pruned (EB Train) ResNet-50 model results with prune ratio pr at $30\%, 50\%, 70\%$ over the ImageNet dataset

Model architectures	# Parameters	Final Test Acc. (Top-1)	Final Test Acc. (Top-5)	MACs (G)
vanilla ResNet-50	$25,610,205$	75.99%	92.98%	4.12
PUFFERFISH ResNet-50	$15,202,344$	75.62%	92.55%	3.6
EB Train ($pr = 30\%$)	$16,466,787$	73.86%	91.52%	2.8
EB Train ($pr = 50\%$)	$15,081,947$	73.35%	91.36%	2.37
EB Train ($pr = 70\%$)	$7,882,503$	70.16%	89.55%	1.03

2019). To make a fair comparison, we train PUFFERFISH with the same hyper-parameters that EB Train uses, *e.g.*, removing label smoothing and only decaying the learning rate at the 30-th and the 60-th epochs with the factor 0.1.

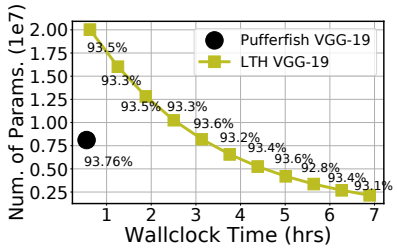

(a) Model size *vs* Runtime

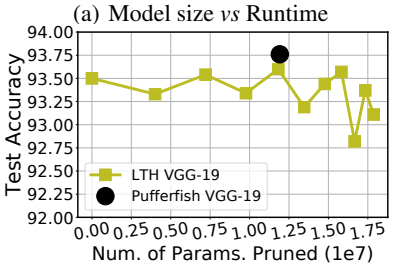

(b) Model size *vs* Test Acc.

Figure 5. The performance comparison between PUFFERFISH and LTH over a VGG-19 model trained over the CIFAR-10 dataset: (a) the number of parameters *v.s.* wall-clock runtime; (b) the number of parameters pruned *v.s.* the test accuracy.

Comparison with LTH. The recent LTH literature initiated by Frankle et al. (Frankle & Carbin, 2018), indicates that dense, randomly-initialized networks contain sparse subnetworks (referred to as "*winning tickets*") that—when trained in isolation—reach test accuracy comparable to the original network (Frankle & Carbin, 2018). To find the winning tickets, an iterative pruning algorithm is conducted, which trains, prunes, and rewinds the remaining unpruned elements to their original random values repeatedly. Though LTH can compress the model massively without significant accuracy loss, the iterative pruning is computationally heavy. We compare PUFFERFISH to LTH across model sizes and computational costs on VGG-19 trained with CIFAR-10. The results are shown in Figure 5(a), 5(b) where we observe that to prune the same number of parameters, LTH costs $5.67\times$ more time than PUFFERFISH.

Ablation study. We conduct an ablation study on the accuracy loss mitigation methods in PUFFERFISH, *i.e.*, hybrid network and vanilla warm-up training. The results on ResNet-18+CIFAR-10 are shown in Table 8, which indicate that the hybrid network and vanilla warm-up training methods help to mitigate the accuracy loss effectively. Results on the other datasets can be found in the Appendix.

Table 8. The effect of vanilla warm-up training and hybrid network architectures of PUFFERFISH of the low rank ResNet-18 trained over the CIFAR-10 dataset. Results are averaged across 3 independent trials with different random seeds.

Methods	Test Loss	Test Acc. (%)
Low-rank ResNet-18	0.31 ± 0.01	93.75 ± 0.19
Hybrid ResNet-18 (wo. vanilla warm-up)	0.30 ± 0.02	93.92 ± 0.45
Hybrid ResNet-18 (w. vanilla warm-up)	$\mathbf{0.25} \pm 0.01$	$\mathbf{94.87} \pm 0.21$

Limitations of PUFFERFISH. One limitation of PUFFERFISH is that it introduces two extra hyper-parameters, *i.e.*, the initial low-rank layer index K and the vanilla warm-up epoch E_{wu}, hence hyperparameter tuning requires extra effort. Another limitation is that although PUFFERFISH reduces the parameters in ResNet-18 and VGG-19 models effectively for the CIFAR-10 dataset, it only finds $1.68\times$ and $1.72\times$ smaller models for ResNet-50 and WideResNet-50-2 in order to preserve good final model accuracy.

5 CONCLUSION

We propose PUFFERFISH, a communication and computation efficient distributed training framework. Instead of gradient compression, PUFFERFISH trains low-rank networks initialized by factorizing a partially trained full-rank model. The use of a hybrid low-rank model and warm-up training, allows PUFFERFISH to preserve the accuracy of the fully dense SGD trained model, while effectively reducing its size. PUFFERFISH achieves high computation and communication efficiency and completely bypasses the gradient encoding and decoding, while yielding smaller and more accurate models compared pruning methods such the LTH and EB Train, while avoiding the burden of "winning the lottery".

Acknowledgments This research is supported by an NSF CAREER Award #1844951, two SONY Faculty Innovation Awards, an AFOSR & AFRL Center of Excellence Award FA9550-18-1-0166, and an NSF TRIPODS Award #1740707. The authors also thank Yoshiki Tanaka, Hisahiro Suganuma, Pongsakorn U-chupala, Yuji Nishimaki, and Tomoki Sato from SONY for invaluable discussions and feedback.

REFERENCES

Abadi, M., Barham, P., Chen, J., Chen, Z., Davis, A., Dean, J., Devin, M., Ghemawat, S., Irving, G., Isard, M., et al. Tensorflow: A system for large-scale machine learning. In *12th {USENIX} Symposium on Operating Systems Design and Implementation ({OSDI} 16)*, pp. 265–283, 2016.

Achille, A., Rovere, M., and Soatto, S. Critical learning periods in deep networks. In *International Conference on Learning Representations*, 2018.

Agarwal, S., Wang, H., Lee, K., Venkataraman, S., and Papailiopoulos, D. Accordion: Adaptive gradient communication via critical learning regime identification. *arXiv preprint arXiv:2010.16248*, 2020.

Aji, A. F. and Heafield, K. Sparse communication for distributed gradient descent. *arXiv preprint arXiv:1704.05021*, 2017.

Alistarh, D., Grubic, D., Li, J., Tomioka, R., and Vojnovic, M. Qsgd: Communication-efficient SGD via gradient quantization and encoding. In *Advances in Neural Information Processing Systems*, pp. 1707–1718, 2017.

Bernstein, J., Wang, Y.-X., Azizzadenesheli, K., and Anandkumar, A. signsgd: Compressed optimisation for non-convex problems. In *International Conference on Machine Learning*, pp. 560–569, 2018a.

Bernstein, J., Zhao, J., Azizzadenesheli, K., and Anandkumar, A. signsgd with majority vote is communication efficient and fault tolerant. In *International Conference on Learning Representations*, 2018b.

Brown, T. B., Mann, B., Ryder, N., Subbiah, M., Kaplan, J., Dhariwal, P., Neelakantan, A., Shyam, P., Sastry, G., Askell, A., et al. Language models are few-shot learners. *arXiv preprint arXiv:2005.14165*, 2020.

Chen, C.-Y., Choi, J., Brand, D., Agrawal, A., Zhang, W., and Gopalakrishnan, K. Adacomp: Adaptive residual gradient compression for data-parallel distributed training. *arXiv preprint arXiv:1712.02679*, 2017.

Chen, J., Pan, X., Monga, R., Bengio, S., and Jozefowicz, R. Revisiting distributed synchronous SGD. *arXiv preprint arXiv:1604.00981*, 2016a.

Chen, Y.-H., Emer, J., and Sze, V. Eyeriss: A spatial architecture for energy-efficient dataflow for convolutional neural networks. *ACM SIGARCH Computer Architecture News*, 44(3):367–379, 2016b.

Chollet, F. Xception: Deep learning with depthwise separable convolutions. In *Proceedings of the IEEE conference on computer vision and pattern recognition*, pp. 1251–1258, 2017.

De Sa, C., Feldman, M., Ré, C., and Olukotun, K. Understanding and optimizing asynchronous low-precision stochastic gradient descent. In *Proceedings of the 44th Annual International Symposium on Computer Architecture*, pp. 561–574. ACM, 2017.

De Sa, C., Leszczynski, M., Zhang, J., Marzoev, A., Aberger, C. R., Olukotun, K., and Ré, C. High-accuracy low-precision training. *arXiv preprint arXiv:1803.03383*, 2018.

De Sa, C. M., Zhang, C., Olukotun, K., and Ré, C. Taming the wild: A unified analysis of hogwild-style algorithms. In *Advances in neural information processing systems*, pp. 2674–2682, 2015.

Dean, J., Corrado, G., Monga, R., Chen, K., Devin, M., Mao, M., Senior, A., Tucker, P., Yang, K., Le, Q. V., et al. Large scale distributed deep networks. In *Advances in neural information processing systems*, pp. 1223–1231, 2012.

Deng, J., Dong, W., Socher, R., Li, L.-J., Li, K., and Fei-Fei, L. Imagenet: A large-scale hierarchical image database. In *2009 IEEE conference on computer vision and pattern recognition*, pp. 248–255. Ieee, 2009.

Devlin, J., Chang, M.-W., Lee, K., and Toutanova, K. Bert: Pre-training of deep bidirectional transformers for language understanding. *arXiv preprint arXiv:1810.04805*, 2018.

Devlin, J., Chang, M.-W., Lee, K., and Toutanova, K. Bert: Pre-training of deep bidirectional transformers for language understanding. In *Proceedings of the 2019 Conference of the North American Chapter of the Association for Computational Linguistics: Human Language Technologies, Volume 1 (Long and Short Papers)*, pp. 4171–4186, 2019.

Elliott, D., Frank, S., Sima'an, K., and Specia, L. Multi30k: Multilingual english-german image descriptions. *arXiv preprint arXiv:1605.00459*, 2016.

Frankle, J. and Carbin, M. The lottery ticket hypothesis: Finding sparse, trainable neural networks. *arXiv preprint arXiv:1803.03635*, 2018.

Goyal, P., Dollár, P., Girshick, R., Noordhuis, P., Wesolowski, L., Kyrola, A., Tulloch, A., Jia, Y., and He, K. Accurate, large minibatch sgd: Training imagenet in 1 hour. *arXiv preprint arXiv:1706.02677*, 2017.

Grubic, D., Tam, L., Alistarh, D., and Zhang, C. Synchronous multi-GPU deep learning with low-precision communication: An experimental study. 2018.

Han, S., Mao, H., and Dally, W. J. Deep compression: Compressing deep neural networks with pruning, trained quantization and huffman coding. *arXiv preprint arXiv:1510.00149*, 2015.

He, K., Zhang, X., Ren, S., and Sun, J. Deep residual learning for image recognition. In *Proceedings of the IEEE conference on computer vision and pattern recognition*, pp. 770–778, 2016.

He, Y., Zhang, X., and Sun, J. Channel pruning for accelerating very deep neural networks. In *Proceedings of the IEEE International Conference on Computer Vision*, pp. 1389–1397, 2017.

Hochreiter, S. and Schmidhuber, J. Long short-term memory. *Neural computation*, 9(8):1735–1780, 1997.

Howard, A. G., Zhu, M., Chen, B., Kalenichenko, D., Wang, W., Weyand, T., Andreetto, M., and Adam, H. Mobilenets: Efficient convolutional neural networks for mobile vision applications. *arXiv preprint arXiv:1704.04861*, 2017.

Hu, H., Peng, R., Tai, Y.-W., and Tang, C.-K. Network trimming: A data-driven neuron pruning approach towards efficient deep architectures. *arXiv preprint arXiv:1607.03250*, 2016.

Huang, G., Liu, Z., Weinberger, K. Q., and van der Maaten, L. Densely connected convolutional networks. In *Proceedings of the IEEE conference on computer vision and pattern recognition*, volume 1, pp. 3, 2017.

Hubara, I., Courbariaux, M., Soudry, D., El-Yaniv, R., and Bengio, Y. Binarized neural networks. In *Advances in neural information processing systems*, pp. 4107–4115, 2016.

Hubara, I., Courbariaux, M., Soudry, D., El-Yaniv, R., and Bengio, Y. Quantized neural networks: Training neural networks with low precision weights and activations. *The Journal of Machine Learning Research*, 18(1):6869–6898, 2017.

Iandola, F. N., Han, S., Moskewicz, M. W., Ashraf, K., Dally, W. J., and Keutzer, K. Squeezenet: Alexnet-level accuracy with 50x fewer parameters and¡ 0.5 mb model size. *arXiv preprint arXiv:1602.07360*, 2016.

Idelbayev, Y. and Carreira-Perpinán, M. A. Low-rank compression of neural nets: Learning the rank of each layer. In *Proceedings of the IEEE/CVF Conference on Computer Vision and Pattern Recognition*, pp. 8049–8059, 2020.

Ioannou, Y., Robertson, D., Shotton, J., Cipolla, R., and Criminisi, A. Training cnns with low-rank filters for efficient image classification. *arXiv preprint arXiv:1511.06744*, 2015.

Ioffe, S. and Szegedy, C. Batch normalization: Accelerating deep network training by reducing internal covariate shift. *arXiv preprint arXiv:1502.03167*, 2015.

Jaderberg, M., Vedaldi, A., and Zisserman, A. Speeding up convolutional neural networks with low rank expansions. *arXiv preprint arXiv:1405.3866*, 2014.

Jastrzebski, S., Szymczak, M., Fort, S., Arpit, D., Tabor, J., Cho, K., and Geras, K. The break-even point on optimization trajectories of deep neural networks. *arXiv preprint arXiv:2002.09572*, 2020.

Jiang, Y., Zhu, Y., Lan, C., Yi, B., Cui, Y., and Guo, C. A unified architecture for accelerating distributed {DNN} training in heterogeneous gpu/cpu clusters. In *14th {USENIX} Symposium on Operating Systems Design and Implementation ({OSDI} 20)*, pp. 463–479, 2020.

Karimireddy, S. P., Rebjock, Q., Stich, S., and Jaggi, M. Error feedback fixes signsgd and other gradient compression schemes. In *International Conference on Machine Learning*, pp. 3252–3261, 2019.

Keskar, N. S., Mudigere, D., Nocedal, J., Smelyanskiy, M., and Tang, P. T. P. On large-batch training for deep learning: Generalization gap and sharp minima. *arXiv preprint arXiv:1609.04836*, 2016.

Konečnỳ, J. and Richtárik, P. Randomized distributed mean estimation: Accuracy vs communication. *arXiv preprint arXiv:1611.07555*, 2016.

Konečnỳ, J., McMahan, H. B., Yu, F. X., Richtárik, P., Suresh, A. T., and Bacon, D. Federated learning: Strategies for improving communication efficiency. *arXiv preprint arXiv:1610.05492*, 2016.

Krizhevsky, A., Hinton, G., et al. Learning multiple layers of features from tiny images. 2009.

Lan, Z., Chen, M., Goodman, S., Gimpel, K., Sharma, P., and Soricut, R. Albert: A lite bert for self-supervised learning of language representations. *arXiv preprint arXiv:1909.11942*, 2019.

Leblond, R., Pedregosa, F., and Lacoste-Julien, S. ASAGA: asynchronous parallel SAGA. *arXiv preprint arXiv:1606.04809*, 2016.

Leclerc, G. and Madry, A. The two regimes of deep network training. *arXiv preprint arXiv:2002.10376*, 2020.

Li, H., Kadav, A., Durdanovic, I., Samet, H., and Graf, H. P. Pruning filters for efficient convnets. *arXiv preprint arXiv:1608.08710*, 2016.

Li, M., Andersen, D. G., Park, J. W., Smola, A. J., Ahmed, A., Josifovski, V., Long, J., Shekita, E. J., and Su, B.-Y. Scaling distributed machine learning with the parameter server. *OSDI*, 1(10.4):3, 2014.

Lin, M., Chen, Q., and Yan, S. Network in network. *arXiv preprint arXiv:1312.4400*, 2013.

Lin, Y., Han, S., Mao, H., Wang, Y., and Dally, W. J. Deep gradient compression: Reducing the communication bandwidth for distributed training. *arXiv preprint arXiv:1712.01887*, 2017.

Liu, Z., Sun, M., Zhou, T., Huang, G., and Darrell, T. Rethinking the value of network pruning. *arXiv preprint arXiv:1810.05270*, 2018.

Luo, J.-H., Wu, J., and Lin, W. Thinet: A filter level pruning method for deep neural network compression. In *Proceedings of the IEEE international conference on computer vision*, pp. 5058–5066, 2017.

Mania, H., Pan, X., Papailiopoulos, D., Recht, B., Ramchandran, K., and Jordan, M. I. Perturbed iterate analysis for asynchronous stochastic optimization. *arXiv preprint arXiv:1507.06970*, 2015.

Merity, S., Xiong, C., Bradbury, J., and Socher, R. Pointer sentinel mixture models. *arXiv preprint arXiv:1609.07843*, 2016.

Paszke, A., Gross, S., Massa, F., Lerer, A., Bradbury, J., Chanan, G., Killeen, T., Lin, Z., Gimelshein, N., Antiga, L., et al. Pytorch: An imperative style, high-performance deep learning library. In *Advances in neural information processing systems*, pp. 8026–8037, 2019.

Press, O. and Wolf, L. Using the output embedding to improve language models. *arXiv preprint arXiv:1608.05859*, 2016.

Qi, H., Sparks, E. R., and Talwalkar, A. Paleo: A performance model for deep neural networks. In *Proceedings of the International Conference on Learning Representations*, 2017.

Rastegari, M., Ordonez, V., Redmon, J., and Farhadi, A. Xnor-net: Imagenet classification using binary convolutional neural networks. In *European conference on computer vision*, pp. 525–542. Springer, 2016.

Renggli, C., Alistarh, D., and Hoefler, T. SparCML: high-performance sparse communication for machine learning. *arXiv preprint arXiv:1802.08021*, 2018.

Sainath, T. N., Kingsbury, B., Sindhwani, V., Arisoy, E., and Ramabhadran, B. Low-rank matrix factorization for deep neural network training with high-dimensional output targets. In *Acoustics, Speech and Signal Processing (ICASSP), 2013 IEEE International Conference on*, pp. 6655–6659. IEEE, 2013.

Seide, F., Fu, H., Droppo, J., Li, G., and Yu, D. 1-bit stochastic gradient descent and its application to data-parallel distributed training of speech dnns. In *Fifteenth Annual Conference of the International Speech Communication Association*, 2014.

Simonyan, K. and Zisserman, A. Very deep convolutional networks for large-scale image recognition. *arXiv preprint arXiv:1409.1556*, 2014.

Stich, S. U., Cordonnier, J.-B., and Jaggi, M. Sparsified sgd with memory. In *Advances in Neural Information Processing Systems*, pp. 4447–4458, 2018.

Strom, N. Scalable distributed DNN training using commodity gpu cloud computing. In *Sixteenth Annual Conference of the International Speech Communication Association*, 2015.

Suresh, A. T., Yu, F. X., Kumar, S., and McMahan, H. B. Distributed mean estimation with limited communication. *arXiv preprint arXiv:1611.00429*, 2016.

Tan, M. and Le, Q. V. Efficientnet: Rethinking model scaling for convolutional neural networks. *arXiv preprint arXiv:1905.11946*, 2019.

Tang, H., Yu, C., Lian, X., Zhang, T., and Liu, J. Doublesqueeze: Parallel stochastic gradient descent with double-pass error-compensated compression. In *International Conference on Machine Learning*, pp. 6155–6165. PMLR, 2019.

Thakur, R., Rabenseifner, R., and Gropp, W. Optimization of collective communication operations in mpich. *The International Journal of High Performance Computing Applications*, 19(1):49–66, 2005.

Touvron, H., Vedaldi, A., Douze, M., and Jégou, H. Fixing the train-test resolution discrepancy: Fixefficientnet. *arXiv preprint arXiv:2003.08237*, 2020.

Tsuzuku, Y., Imachi, H., and Akiba, T. Variance-based gradient compression for efficient distributed deep learning. *arXiv preprint arXiv:1802.06058*, 2018.

Tucker, L. R. Some mathematical notes on three-mode factor analysis. *Psychometrika*, 31(3):279–311, 1966.

Vaswani, A., Shazeer, N., Parmar, N., Uszkoreit, J., Jones, L., Gomez, A. N., Kaiser, Ł., and Polosukhin, I. Attention is all you need. In *Advances in neural information processing systems*, pp. 5998–6008, 2017.

Vogels, T., Karimireddy, S. P., and Jaggi, M. Powersgd: Practical low-rank gradient compression for distributed optimization. In *Advances in Neural Information Processing Systems*, pp. 14259–14268, 2019.

Waleffe, R. and Rekatsinas, T. Principal component networks: Parameter reduction early in training. *arXiv preprint arXiv:2006.13347*, 2020.

Wang, H., Sievert, S., Liu, S., Charles, Z., Papailiopoulos, D., and Wright, S. Atomo: Communication-efficient learning via atomic sparsification. In *Advances in Neural Information Processing Systems*, pp. 9850–9861, 2018.

Wen, W., Wu, C., Wang, Y., Chen, Y., and Li, H. Learning structured sparsity in deep neural networks. In *Advances in neural information processing systems*, pp. 2074–2082, 2016.

Wen, W., Xu, C., Yan, F., Wu, C., Wang, Y., Chen, Y., and Li, H. Terngrad: Ternary gradients to reduce communication in distributed deep learning. In *Advances in Neural Information Processing Systems*, pp. 1508–1518, 2017.

Wiesler, S., Richard, A., Schluter, R., and Ney, H. Mean-normalized stochastic gradient for large-scale deep learning. In *Acoustics, Speech and Signal Processing (ICASSP), 2014 IEEE International Conference on*, pp. 180–184. IEEE, 2014.

Wu, J., Leng, C., Wang, Y., Hu, Q., and Cheng, J. Quantized convolutional neural networks for mobile devices. In *Proceedings of the IEEE Conference on Computer Vision and Pattern Recognition*, pp. 4820–4828, 2016.

Wu, J., Huang, W., Huang, J., and Zhang, T. Error compensated quantized sgd and its applications to large-scale distributed optimization. In *International Conference on Machine Learning*, pp. 5325–5333, 2018.

Xue, J., Li, J., and Gong, Y. Restructuring of deep neural network acoustic models with singular value decomposition. In *Interspeech*, pp. 2365–2369, 2013.

Yang, T.-J., Chen, Y.-H., and Sze, V. Designing energy-efficient convolutional neural networks using energy-aware pruning. In *Proceedings of the IEEE Conference on Computer Vision and Pattern Recognition*, pp. 5687–5695, 2017.

You, H., Li, C., Xu, P., Fu, Y., Wang, Y., Chen, X., Baraniuk, R. G., Wang, Z., and Lin, Y. Drawing early-bird tickets: Towards more efficient training of deep networks. *arXiv preprint arXiv:1909.11957*, 2019.

Yu, J., Yang, L., Xu, N., Yang, J., and Huang, T. Slimmable neural networks. *arXiv preprint arXiv:1812.08928*, 2018a.

Yu, R., Li, A., Chen, C.-F., Lai, J.-H., Morariu, V. I., Han, X., Gao, M., Lin, C.-Y., and Davis, L. S. Nisp: Pruning networks using neuron importance score propagation. In *Proceedings of the IEEE Conference on Computer Vision and Pattern Recognition*, pp. 9194–9203, 2018b.

Zagoruyko, S. and Komodakis, N. Wide residual networks. *arXiv preprint arXiv:1605.07146*, 2016.

Zhang, H., Li, J., Kara, K., Alistarh, D., Liu, J., and Zhang, C. Zipml: Training linear models with end-to-end low precision, and a little bit of deep learning. In *International Conference on Machine Learning*, pp. 4035–4043, 2017.

Zhang, X., Zhou, X., Lin, M., and Sun, J. Shufflenet: An extremely efficient convolutional neural network for mobile devices. In *Proceedings of the IEEE conference on computer vision and pattern recognition*, pp. 6848–6856, 2018.

Zhou, A., Yao, A., Guo, Y., Xu, L., and Chen, Y. Incremental network quantization: Towards lossless cnns with low-precision weights. *arXiv preprint arXiv:1702.03044*, 2017.

Zhou, D., Ye, M., Chen, C., Meng, T., Tan, M., Song, X., Le, Q., Liu, Q., and Schuurmans, D. Go wide, then narrow: Efficient training of deep thin networks. *arXiv preprint arXiv:2007.00811*, 2020.

Zhou, S., Wu, Y., Ni, Z., Zhou, X., Wen, H., and Zou, Y. DoReFa-Net: training low bitwidth convolutional neural networks with low bitwidth gradients. *arXiv preprint arXiv:1606.06160*, 2016.

Zhu, C., Han, S., Mao, H., and Dally, W. J. Trained ternary quantization. *arXiv preprint arXiv:1612.01064*, 2016.

Zhu, M. and Gupta, S. To prune, or not to prune: exploring the efficacy of pruning for model compression. *arXiv preprint arXiv:1710.01878*, 2017.

A SOFTWARE VERSIONS USED IN THE EXPERIMENTS

Since we provide wall-clock time results, it is important to specify the versions of the libraries we used. For the full-precision (FP32) results, we used the `pytorch_p36` virtual environment associated with the "Deep Learning AMI (Ubuntu 18.04) Version 40.0 (ami-084f81625fbc98fa4)" on Amazon EC2, *i.e.*, `PyTorch 1.4.0` with CUDA10.1.243. Since AMP is only supported after 1.6.0 of PyTorch, we use `PyTorch 1.6.0` with CUDA 10.1.

B DETAILED DISCUSSION ON THE COMPUTATION COMPLEXITY OF VARIOUS LAYERS

We provide the computational complexity and number of parameters in the vanilla and low-rank factorized layers returned by PUFFERFISH in Section 2. We provide a more detailed discussion here. For the number of parameters, we do not count the bias terms.

FC layer. We start from the FC layer. Assuming the input and the vanilla and low-rank FC weights are with dimensions $x \in \mathbb{R}^m, W \in \mathbb{R}^{m\times n}, U \in \mathbb{R}^{m\times r}, V^\top \in \mathbb{R}^{r\times n}$, the computation complexity is simply $\mathcal{O}(mn)$ for xW and $\mathcal{O}(mr+rn)$ for $(xU)V^\top$. For the number of parameters, the vanilla FC layer contains mn parameters in total while the low-rank FC layer contains $r(m+n)$ parameters in total.

Convolution layer. For a convolution layer, assuming the input is with dimension $x \in \mathbb{R}^{c_{\text{in}}\times H\times W}$ (the input "image" has c_{in} color channels and with size $H \times W$), the computation complexity of a vanilla convolution layer with weight $W \in \mathbb{R}^{c_{\text{in}}\times c_{\text{out}}\times k\times k}$ is $\mathcal{O}(c_{\text{in}}c_{\text{out}}k^2HW)$ for computing $W * x$ where $*$ is the linear convolution operation. And the low-rank factorized convolution layer with dimension $U \in \mathbb{R}^{c_{\text{in}}\times r\times k\times k}, V \in \mathbb{R}^{r\times c_{\text{out}}\times 1\times 1}$ has the computation complexity at $\mathcal{O}(rc_{\text{in}}k^2HW)$ for $U * x$ and $\mathcal{O}(rHWc_{\text{out}})$ for convolving the output of $U * x$ with V. For the number of parameters, the vanilla convolution layer contains $c_{\text{in}}c_{\text{out}}k^2$ parameters in total while the low-rank convolution layer contains $c_{\text{in}}rk^2 + rc_{\text{out}}$ parameters in total.

LSTM layer. For the LSTM layer, the computation complexity is similar to the computation complexity of the FC layer. Assuming the tokenized input is with dimension $x \in \mathbb{R}^d$, and the concatenated input-hidden and hidden-hidden weights $W_i \in \mathbb{R}^{d\times 4h}, W_h \in \mathbb{R}^{4h\times h}$, thus the computation complexity of the forward propagation of a LSTM layer is $\mathcal{O}(4dh + 4h^2)$. And for the low-rank LSTM layer, the computation complexity becomes $\mathcal{O}(dr + 4rh + 4hr + rh)$ (as mentioned in Section 2, we assume that the same rank r is used for both the input-hidden weight and hidden-hidden weight). For the number of parameters, the vanilla LSTM layer contains $4dh + 4h^2$ parameters in total while the low-rank convolution layer contains $4(dr + rh) + 4(hr + rh) = 4dr + 12hr$ parameters in total.

Transformer. For the encoder layer in the Transformer architecture, there are two main components, *i.e.*, the multi-head attention layer and the FFN layer. Note that, for the multi-head attention layer, the dimensions of the projection matrices are: The dimensions of the matrices are $Q, K, V \in \mathbb{R}^{n\times pd}, W^Q, W^K, W^V \in \mathbb{R}^{pd\times d}, W^O \in \mathbb{R}^{pd\times pd}$. And the dimensions of the two FC layers in the FFN are with dimensions $W_1 \in \mathbb{R}^{pd\times 4pd}, W_2 \in \mathbb{R}^{4pd\times pd}$. And we assume a sequence of input tokens with length N is batched to process together. Since the computation for each attention head is computed independently, we only analyze the computation complexity of a single head attention, which is $\mathcal{O}\big(\underbrace{d\cdot pd\cdot N}_{\text{proj. of } Q,K,V} + \underbrace{2N^2\cdot d}_{\text{attention layer}} + \underbrace{pd\cdot pd\cdot N}_{\text{proj. of the output of attention}}\big) = \mathcal{O}\big((p+p^2)Nd^2 + N^2d\big) = \mathcal{O}\big(Np^2d^2 + N^2d\big)$. Similarly, the computation complexity for the FFN layer is $\mathcal{O}\big(\underbrace{4\times p^2d^2N}_{xW_1} + \underbrace{4\times p^2d^2N}_{xW_1W_2}\big)$. For the low-rank attention layer, the computation complexity becomes $\mathcal{O}\big(\underbrace{(dr+rpd)\cdot N}_{\text{low-rank proj.}} + \underbrace{(pdr+rpd)\cdot N}_{\text{low-rank proj. of the output}} + 2N^2\cdot d\big) = \mathcal{O}\big((p+1)drN + 2Ndpr + 2N^2d\big) = \mathcal{O}\big(pdrN + N^2d\big)$ and the computation complexity for FFN $\mathcal{O}\big(\underbrace{(p\cdot d\cdot r + 4r\cdot h\cdot d)\cdot N}_{xW_1} + \underbrace{(p\cdot d\cdot r + 4r\cdot p\cdot d)\cdot N}_{xW_1W_2}\big)$. For the number of parameters, the vanilla multi-head attention layer contains $3pd^2\cdot p + p^2d^2 = 4p^2d^2$ parameters in total while the low-rank multi-head attention layer contains $3p(pdr+rd)+(pdr+rpd) = prd(3p+5)$ parameters in total. The vanilla FFN layer contains $4p^2d^2+4p^2d^2 = 8p^2d^2$ parameters in total while the low-rank FFN layer contains $(pdr + r4pd) + (4pdr + rpd) = 10pdr$ parameters in total.

C DETAILS ON THE DATASET AND MODELS USED FOR THE EXPERIMENT

The details of the datasets used in the experiments are summarized in Table 9.

D DETAILS ON THE HYBRID NETWORKS IN THE EXPERIMENTS

The hybrid VGG-19-BN architecture. we found that using $K = 10$ in the VGG-19-BN architecture leads to good test accuracy and moderate model compression ratio.

Table 9. The datasets used and their associated learning models.

Method	CIFAR-10	ImageNet	WikiText-2	WMT16' Gen-Eng
# Data points	$60,000$	$1,281,167$	$29,000$	$1,017,981$
Data Dimension	$32 \times 32 \times 3$	$224 \times 224 \times 3$	$1,500$	$9,521$
Model	VGG-19-BN;ResNet-18	ResNet-50;WideResNet-50-2	2 layer LSTM	Transformer ($p = 8, N = 6$)
Optimizer	SGD		SGD	ADAM
Hyper-params.	Init lr: 0.01		lr: 20(decay with 0.25 when val. loss not decreasing)	Init lr: 0.001
	momentum: 0.9, ℓ_2 weight decay: 10^{-4}		grad. norm clipping 0.25	$\beta s = (0.9, 0.98), \epsilon = 10^{-8}$

Table 10. Detailed information of the hybrid VGG-19-BN architecture used in our experiments, all non-linear activation function in this architecture is ReLU after each convolution layer (omitted in the Table). The shapes for convolution layers follows (c_{in}, c_{out}, k, k). There is a BatchNorm layer after each convolution layer with number of neurons the same as c_{out} (also omitted in the Table).

Parameter	Shape	Layer hyper-parameter
layer1.conv1.weight	$3 \times 64 \times 3 \times 3$	stride:1;padding:1
layer2.conv2.weight	$64 \times 64 \times 3 \times 3$	stride:1;padding:1
pooling.max	N/A	kernel size:2;stride:2
layer3.conv3.weight	$64 \times 128 \times 3 \times 3$	stride:1;padding:1
layer4.conv4.weight	$128 \times 128 \times 3 \times 3$	stride:1;padding:1
pooling.max	N/A	kernel size:2;stride:2
layer5.conv5.weight	$128 \times 256 \times 3 \times 3$	stride:1;padding:1
layer6.conv6.weight	$256 \times 256 \times 3 \times 3$	stride:1;padding:1
layer7.conv7.weight	$256 \times 256 \times 3 \times 3$	stride:1;padding:1
layer8.conv8.weight	$256 \times 256 \times 3 \times 3$	stride:1;padding:1
pooling.max	N/A	kernel size:2;stride:2
layer9.conv9.weight	$256 \times 512 \times 3 \times 3$	stride:1;padding:1
layer10.conv10_u.weight	$512 \times 128 \times 3 \times 3$	stride:1;padding:1
layer10.conv10_v.weight	$128 \times 512 \times 1 \times 1$	stride:1
layer11.conv11_u.weight	$512 \times 128 \times 3 \times 3$	stride:1;padding:1
layer11.conv11_v.weight	$128 \times 512 \times 1 \times 1$	stride:1
layer12.conv12_u.weight	$512 \times 128 \times 3 \times 3$	stride:1;padding:1
layer12.conv12_v.weight	$128 \times 512 \times 1 \times 1$	stride:1
pooling.max	N/A	kernel size:2;stride:2
layer13.conv13_u.weight	$512 \times 128 \times 3 \times 3$	stride:1;padding:1
layer13.conv13_v.weight	$128 \times 512 \times 1 \times 1$	stride:1
layer14.conv14_u.weight	$512 \times 128 \times 3 \times 3$	stride:1;padding:1
layer14.conv14_v.weight	$128 \times 512 \times 1 \times 1$	stride:1
layer15.conv15_u.weight	$512 \times 128 \times 3 \times 3$	stride:1;padding:1
layer15.conv15_v.weight	$128 \times 512 \times 1 \times 1$	stride:1
layer16.conv16_u.weight	$512 \times 128 \times 3 \times 3$	stride:1;padding:1
layer16.conv16_v.weight	$128 \times 512 \times 1 \times 1$	stride:1
pooling.max	N/A	kernel size:2;stride:2
layer17.fc17.weight	512×512	N/A
layer17.fc17.bias	512	N/A
layer18.fc18.weight	512×512	N/A
layer18.fc18.bias	512	N/A
layer19.fc19.weight	512×10	N/A
layer19.fc19.bias	10	N/A

The low-rank LSTM architecture. Note that we only use a 2-layer stacked LSTM as the model in the WikiText-2 next word prediction task. Our implementation is directly modified from the PyTorch original example [4]. We used the tied version of LSTM, *i.e.*, enabling weight sharing for the encode embedding and decode embedding layers.

Table 11. Detailed information on the low-rank LSTM architecture in our experiment.

Parameter	Shape	Hyper-param.
encoder.weight	33278×1500	N/A
dropout	N/A	$p = 0.65$
lstm0.weight.ii/f/g/o_u	1500×375	N/A
lstm0.weight.ii/f/g/o_v	375×1500	N/A
lstm0.weight.hi/f/g/o_u	1500×375	N/A
lstm0.weight.hi/f/g/o_v	375×1500	N/A
dropout	N/A	$p = 0.65$
lstm1.weight.ii/f/g/o_u	1500×375	N/A
lstm1.weight.ii/f/g/o_v	375×1500	N/A
lstm1.weight.hi/f/g/o_u	1500×375	N/A
lstm1.weight.hi/f/g/o_v	375×1500	N/A
decoder.weight(shared)	1500×33278	N/A

The hybrid ResNet-18, ResNet-50, WideResNet-50-2 architectures. For the CIFAR-10 dataset, we modified the original ResNet-50 architecture described in the original ResNet paper (He et al., 2016). The details about the modified ResNet-18 architecture for the CIFAR-10 dataset are shown in Table 12. The network architecture is modified from the public code repository [5]. For the first 2 convolution block, *i.e.*, conv2_x, we used stride at 1 and padding at 1 for all the convolution layers. For conv3_x, conv4_x, and conv5_x we used the stride at 2 and padding at 1. We also note that there is a BatchNorm layer after each convolution layer with the number of elements equals the number of

[4] https://github.com/pytorch/examples/tree/master/word_language_model

[5] https://github.com/kuangliu/pytorch-cifar

convolution filters. As shown in Table 12, our hybrid architecture starts from the 2nd convolution block, *i.e.*, $K = 4$. Our experimental study generally shows that this choice of hybrid ResNet-18 architecture leads to a good balance between the final model accuracy and the number of parameters. Moreover, we do not handle the downsampling weights in the convolution blocks.

Layer Name	ResNet-18	Rank Information
conv1	3×3, 64, stride 1, padding 1	full-rank
conv2_x	$\begin{bmatrix} 3\times3, 64 \\ 3\times3, 64 \end{bmatrix}\times2$	1st block full-rank 2nd block low-rank conv_u $(64, 16, 3, 3)$, conv_v$(16, 64, 1, 1)$
conv3_x	$\begin{bmatrix} 3\times3, 128 \\ 3\times3, 128 \end{bmatrix}\times2$	low-rank conv_u $(128, 32, 3, 3)$ conv_v $(32, 128, 1, 1)$
conv4_x	$\begin{bmatrix} 3\times3, 256 \\ 3\times3, 256 \end{bmatrix}\times2$	low-rank conv_u $(256, 64, 3, 3)$ conv_v $(64, 256, 1, 1)$
conv5_x	$\begin{bmatrix} 3\times3, 512 \\ 3\times3, 512 \end{bmatrix}\times2$	low-rank conv_u $(512, 128, 3, 3)$ conv_v $(128, 512, 1, 1)$
	Avg Pool, 10-dim FC, SoftMax	

Table 12. The hybrid ResNet-18 architecture for the CIFAR-10 dataset used in the experiments.

For the ResNet-50 architecture, the detailed information is shown in the Table 13. As we observed that the last three convolution blocks, *i.e.*, conv5_x contains around 60% of the total number of parameters in the entire network. Thus, we just factorize the last three convolution blocks and leave all other convolution blocks as full-rank blocks. Note that, different from the ResNet-18 architecture for the CIFAR-10 dataset described above. We also handle the downsampling layer weights inside the ResNet-50 network, which only contains in the very first convolution block of conv5_x. The original dimension of the downsample weight is with shape $(1024, 2048, 1, 1)$. Our factorization strategy leads to the shape of conv_u: $(1024, 256, 1, 1)$ and conv_v: $(256, 2048, 1, 1)$.

Layer Name	output size	ResNet-50	Rank Information
conv1	112×112	7×7, 64, stride 2	full-rank
		3×3 max pool, stride 2	
conv2_x	56×56	$\begin{bmatrix} 1\times1, 64 \\ 3\times3, 64 \\ 1\times1, 256 \end{bmatrix}\times3$	all blocks full-rank
conv3_x	28×28	$\begin{bmatrix} 1\times1, 128 \\ 3\times3, 128 \\ 1\times1, 512 \end{bmatrix}\times4$	all blocks full-rank
conv4_x	14×14	$\begin{bmatrix} 1\times1, 256 \\ 3\times3, 256 \\ 1\times1, 1024 \end{bmatrix}\times6$	all blocks full-rank
conv5_x	7×7	$\begin{bmatrix} 1\times1, 512 \\ 3\times3, 512 \\ 1\times1, 2048 \end{bmatrix}\times3$	conv_1_u $(c_{\text{in}}, \frac{c_{\text{in}}}{4}, 1, 1)$; conv_1_v $(\frac{c_{\text{in}}}{4}, 512, 1, 1)$ conv_2_u $(512, 128, 3, 3)$; conv_2_v $(128, 512, 1, 1)$ conv_3_u $(512, 128, 1, 1)$; conv_2_v $(128, 2048, 1, 1)$
	1×1	Avg pool, 1000-dim FC, SoftMax	

Table 13. The hybrid ResNet-50 architecture for the ImageNet dataset used in the experiments.

For the WideResNet-50, the detailed hybrid architecture we used is shown in Table 14. Similar to our hybrid ResNet-50 architecture, we just factorize the last three convolution blocks and leave all other convolution blocks as full-rank blocks. We also handle the downsampling layer weights inside the WideResNet-50 network, which only contains the very first convolution block of conv5_x. The original dimension of the downsample weight is with shape $(1024, 2048, 1, 1)$. Our factorization strategy leads to the shape of conv_u: $(1024, 256, 1, 1)$ and conv_v: $(256, 2048, 1, 1)$.

Layer Name	output size	WideResNet-50-2	Rank Information
conv1	112×112	7×7, 64, stride 2	full-rank
		3×3 max pool, stride 2	
conv2_x	56×56	$\begin{bmatrix} 1\times1, 128 \\ 3\times3, 128 \\ 1\times1, 256 \end{bmatrix}\times3$	all blocks full-rank
conv3_x	28×28	$\begin{bmatrix} 1\times1, 256 \\ 3\times3, 256 \\ 1\times1, 512 \end{bmatrix}\times4$	all blocks full-rank
conv4_x	14×14	$\begin{bmatrix} 1\times1, 512 \\ 3\times3, 512 \\ 1\times1, 1024 \end{bmatrix}\times6$	all blocks full-rank
conv5_x	7×7	$\begin{bmatrix} 1\times1, 1024 \\ 3\times3, 1024 \\ 1\times1, 2048 \end{bmatrix}\times3$	conv_1_u $(c_{\text{in}}, \frac{c_{\text{in}}}{4}, 1, 1)$; conv_1_v $(\frac{c_{\text{in}}}{4}, 1024, 1, 1)$ conv_2_u $(1024, 256, 3, 3)$; conv_2_v $(256, 1024, 1, 1)$ conv_3_u $(1024, 256, 1, 1)$; conv_2_v $(256, 2048, 1, 1)$
	1×1	Avg pool, 1000-dim FC, SoftMax	

Table 14. The hybrid WideResNet-50-2 architecture for the ImageNet dataset used in the experiments.

The hybrid Transformer architecture. The Transformer architecture used in the experiment follows from the original Transformer paper (Vaswani et al., 2017). Our implementation is modified from the public code repository [6]. We use the stack of $N = 6$ encoder and decoder layers inside the Transformer architecture and number of head $p = 8$. Since the encoder and decoder layers are identical across the entire architecture, we describe the detailed encoder and decoder architecture information in Table 15 and Table 16. For the hybrid architecture used in the Transformer architecture, we put the very first encoder layer and first decoder layer as full-rank layers, and all other layers are low-rank layers. For low-rank encoder and decoder layers, we used the rank ratio at $\frac{1}{4}$, thus the shape of $U^Q, U^K, U^V, U^O \in \mathbb{R}^{512\times128}, V^{Q\top}, V^{K\top}, V^{V\top}, V^{O\top} \in \mathbb{R}^{128\times512}$. For W_1 in the FFN$(\cdot)$ layer, the $U_1 \in \mathbb{R}^{512\times128}, V_1^\top \in \mathbb{R}^{128\times2048}$. For W_2 in the FFN$(\cdot)$ layer, the $U_2 \in \mathbb{R}^{2048\times128}, V_1^\top \in \mathbb{R}^{128\times512}$.

[6] https://github.com/jadore801120/attention-is-all-you-need-pytorch

Table 15. Detailed information of the encoder layer in the Transformer architecture in our experiment

Parameter	Shape	Hyper-param.
embedding	9521×512	padding index: 1
positional encoding	N/A	N/A
dropout	N/A	$p = 0.1$
encoder.self-attention.wq(W^Q)	512×512	N/A
encoder.self-attention.wk(W^K)	512×512	N/A
encoder.self-attention.wv(W^V)	512×512	N/A
encoder.self-attention.wo(W^O)	512×512	N/A
encoder.self-attention.dropout	N/A	$p = 0.1$
encoder.self-attention.layernorm	512	$\epsilon = 10^{-6}$
encoder.ffn.layer1	512×2048	N/A
encoder.ffn.layer2	2048×512	N/A
encoder.layernorm	512	$\epsilon = 10^{-6}$
dropout	N/A	$p = 0.1$

Table 16. Detailed information of the decoder layer in the Transformer architecture in our experiment

Parameter	Shape	Hyper-param.
embedding	9521×512	padding index: 1
positional encoding	N/A	N/A
dropout	N/A	$p = 0.1$
decoder.self-attention.wq(W^Q)	512×512	N/A
decoder.self-attention.wk(W^K)	512×512	N/A
decoder.self-attention.wv(W^V)	512×512	N/A
decoder.self-attention.wo(W^O)	512×512	N/A
decoder.self-attention.dropout	N/A	$p = 0.1$
decoder.self-attention.layernorm	512	$\epsilon = 10^{-6}$
decoder.enc-attention.wq(W^Q)	512×512	N/A
decoder.enc-attention.wk(W^K)	512×512	N/A
decoder.enc-attention.wv(W^V)	512×512	N/A
decoder.enc-attention.wo(W^O)	512×512	N/A
decoder.enc-attention.dropout	N/A	$p = 0.1$
decoder.enc-attention.layernorm	512	$\epsilon = 10^{-6}$
decoder.ffn.layer1	512×2048	N/A
decoder.ffn.layer2	2048×512	N/A
encoder.layernorm	512	$\epsilon = 10^{-6}$
dropout	N/A	$p = 0.1$

The hybrid VGG-19-BN architecture used for the LTH comparison. To compare PUFFERFISH with LTH, we use the open-source LTH implementation, *i.e.*, https://github.com/facebookresearch/open_lth. The VGG-19-BN model used in the open-source LTH repository is slightly different from the VGG-19-BN architecture described above. We thus use the VGG-19-BN architecture in the LTH code and deploy PUFFERFISH on top of it for fairer comparison. Detailed information about the hybrid VGG-19-BN architecture we used in PUFFERFISH for the comparison with LTH is shown in Table 17.

Table 17. Detailed information of the hybrid VGG-19-BN architecture used in our LTH comparison experiments, all non-linear activation function in this architecture is ReLU after each convolution layer (omitted in the Table). The shapes for convolution layers follows (c_{in}, c_{out}, k, k). There is a BatchNorm layer after each convolution layer with number of neurons the same as c_{out} (also omitted in the Table).

Parameter	Shape	Layer hyper-parameter
layer1.conv1.weight	$3 \times 64 \times 3 \times 3$	stride:1;padding:1
layer2.conv2.weight	$64 \times 64 \times 3 \times 3$	stride:1;padding:1
pooling.max	N/A	kernel size:2;stride:2
layer3.conv3.weight	$64 \times 128 \times 3 \times 3$	stride:1;padding:1
layer4.conv4.weight	$128 \times 128 \times 3 \times 3$	stride:1;padding:1
pooling.max	N/A	kernel size:2;stride:2
layer5.conv5.weight	$128 \times 256 \times 3 \times 3$	stride:1;padding:1
layer6.conv6.weight	$256 \times 256 \times 3 \times 3$	stride:1;padding:1
layer7.conv7.weight	$256 \times 256 \times 3 \times 3$	stride:1;padding:1
layer8.conv8.weight	$256 \times 256 \times 3 \times 3$	stride:1;padding:1
pooling.max	N/A	kernel size:2;stride:2
layer9.conv9.weight	$256 \times 512 \times 3 \times 3$	stride:1;padding:1
layer10.conv10_u.weight	$512 \times 128 \times 3 \times 3$	stride:1;padding:1
layer10.conv10_v.weight	$128 \times 512 \times 1 \times 1$	stride:1
layer11.conv11_u.weight	$512 \times 128 \times 3 \times 3$	stride:1;padding:1
layer11.conv11_v.weight	$128 \times 512 \times 1 \times 1$	stride:1
layer12.conv12_u.weight	$512 \times 128 \times 3 \times 3$	stride:1;padding:1
layer12.conv12_v.weight	$128 \times 512 \times 1 \times 1$	stride:1
pooling.max	N/A	kernel size:2;stride:2
layer13.conv13_u.weight	$512 \times 128 \times 3 \times 3$	stride:1;padding:1
layer13.conv13_v.weight	$128 \times 512 \times 1 \times 1$	stride:1
layer14.conv14_u.weight	$512 \times 128 \times 3 \times 3$	stride:1;padding:1
layer14.conv14_v.weight	$128 \times 512 \times 1 \times 1$	stride:1
layer15.conv15_u.weight	$512 \times 128 \times 3 \times 3$	stride:1;padding:1
layer15.conv15_v.weight	$128 \times 512 \times 1 \times 1$	stride:1
layer16.conv16_u.weight	$512 \times 128 \times 3 \times 3$	stride:1;padding:1
layer16.conv16_v.weight	$128 \times 512 \times 1 \times 1$	stride:1
pooling.max	N/A	kernel size:2;stride:2
layer17.fc17.weight	512×10	N/A
layer17.fc17.bias	10	N/A

E THE COMPATIBILITY OF PUFFERFISH WITH OTHER GRADIENT COMPRESSION METHODS

As PUFFERFISH is a training time parameter reduction method, the gradient of the factorized networks can be compressed further with any gradient compression methods. As POWERSGD is the state-of-the-art gradient compression method and is compatible with `allreduce`, we consider another baseline, *i.e.*, "PUFFERFISH+POWERSGD". We conduct an experimental study over the "PUFFERFISH+POWERSGD" baseline for ResNet-18 trained on CIFAR-10 (results shown in Figure 6). The experiment is running over 8 `p3.2xlarge` EC2 nodes with batch size at 256 per node (2048 in total). The experimental results indicate that combining PUFFERFISH with POWERSGD can effectively reduce the gradient size of PUFFERFISH further, making PUFFERFISH enjoys high computation efficiency and the communication efficiency as high as POWERSGD. However, as POWERSGD conducts layer-wise gradient encoding and decoding on all U_l and V_l layers, the gradient encoding and decoding costs in the "PUFFERFISH+POWERSGD" baseline are higher compared to POWERSGD. We observe that a slightly higher rank is desired when combining PUFFERFISH with POWERSGD to attain good final model accuracy since both model weights and gradients are approximated in this case. In the experimental results shown in Figure 6, we use POWERSGD with rank 4 when combining with PUFFERFISH for both the vanilla warm-up training and the following low-rank training. Moreover, we also found that under the large-batch setting, it is always helpful to re-warmup the learning rate for the "PUFFERFISH+POWERSGD" baseline, *i.e.*, in the first 5 epochs, we warm-up the learning rate linearly from 0.1 to 1.6, then at the 80-th epoch where we switch from the vanilla warm-up training to low-rank training, we conduct the learning rate warm-up again within 5 epochs (from 0.1 to 1.6). Our experimental results suggest that PUFFERFISH can be combined with the gradient compression methods to attain better communication efficiency, but it is desirable to combine PUFFERFISH with the gradient compression methods that can be deployed directly on the fattened gradients, *e.g.*, Top-k.

F DISCUSSION ON THE COMMUNICATION EFFICIENCY OF PUFFERFISH

It is natural to ask the question that "*Why are the previously proposed light weight gradient compression methods slow in practice, e.g., the ones proposed in (Suresh et al., 2016)*?" We agree that there are lots of gradient compression methods, which are computationally cheap. However, other important factors can affect the gradient compression efficiency in practice (taking the gradient compression method

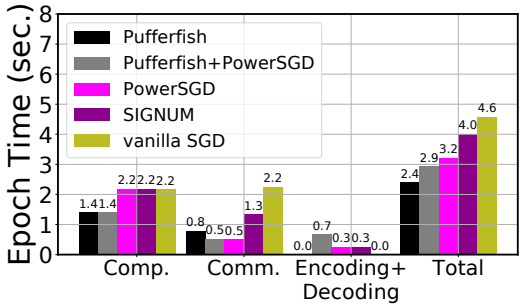

(a) Breakdown per-epoch time

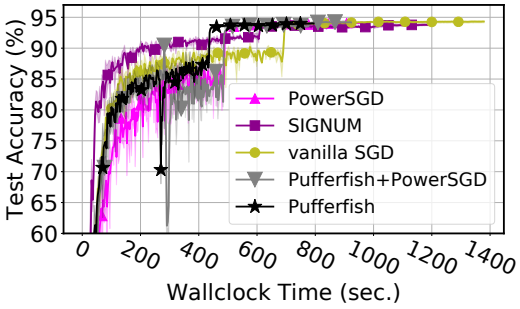

(b) Convergence

Figure 6. (a) Per-epoch breakdown runtime analysis and (b) convergence performance of PUFFERFISH, "PUFFERFISH+POWERSGD (rank 4)", POWERSGD (rank 2), SIGNUM, and vanilla SGD over ResNet-18 trained on the CIFAR-10 dataset.

in (Suresh et al., 2016) as an example):

(i) After the binary sign rounding, extra encoding and decoding steps e.g. binary encoding are required to aggregate the quantized bits to bytes for attaining real communication speedup. That is optimizing the data structures to support low-communication for quantized gradients is necessary for any benefit to the surface, and also quite non trivial. (ii) For most gradient compression schemes, the encoded gradients are not compatible with all-reduce. Thus, all-gather has to be used instead. Unfortunately, in terms of comm. costs all-gather suffers a performance gap that increases with the number of nodes. (iii) In all-reduce, each worker receives a pre-aggregated gradient, making the cost of decompression independent to the number of workers. In all-gather, a worker receives the number of workers compressed gradients that need to be individually decompressed and aggregated. The time for decompression with all-gather therefore scales linearly with the number of workers.

In fact we did run a test for the "*Stochastic binary quantization*" method in (Suresh et al., 2016) on ResNet-50+ImageNet over 16 EC2 `p3.2xlarge` nodes (per node batch size 32) as it is the computationally cheapest methods proposed in the paper. Though it is showed that conducting random rotation over the gradients can improve the compression error, we only care about the computational and communication efficiencies of the method in this particu-

lar experiment. Per epoch runtime results are shown in Figure 7.

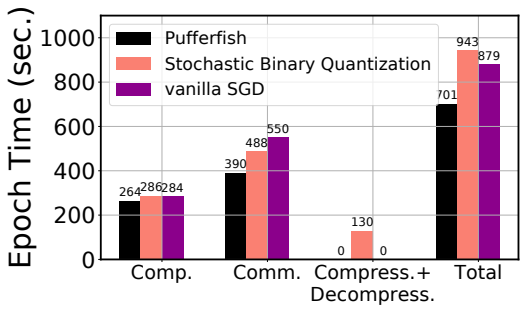

Figure 7. Breakdown per-epoch runtime comparison between PUFFERFISH, vanilla SGD, and stochastic binary quantization.

Note that in the "compress.+decompress." stage, stochastic binary quantization takes 12.1 ± 0.6 seconds for gradient compression and 118.4 ± 0.1 for gradient decompression. We observe that although the stochastic binary quantization is efficient in the compression stage, its gradient decompression cost is expensive. Moreover, all-gather is less efficient compared to all-reduce at the scale of 16 nodes.

G THE EFFECTIVENESS OF USING SVD TO FIND THE LOW-RANK FACTORIZATION

In the vanilla warm-up training strategy proposed in PUFFERFISH, we decompose the network weights using SVD to find the initialization weights for the hybrid network. Though SVD is a computationally expensive method, PUFFERFISH only requires conducting the factorization over the network weights **once** during the entire training process. We explicitly test the overhead incurred by conducting SVD over the model weights here. All the runtimes are measured over the `p3.2xlarge` instance of Amazon EC2 (equipped with Tesla V100 GPU). The results are shown in Figure 18. From the results, it can be observed that the run time on using SVD to factorize the partially trained vanilla full-rank network is quite fast, *e.g.*, on average it only costs 2.2972 seconds over the ResNet-50 trained over the ImageNet dataset.

H DETAILS OF DATA PREPROCESSING

The CIFAR-10 dataset. In preprocessing the images in CIFAR-10 dataset, we follow the standard data augmentation and normalization process. For data augmentation, random cropping and horizontal random flipping are used. Each color channels are normalized with mean and standard deviation by $\mu_r = 0.491, \mu_g = 0.482, \mu_b = 0.447$, $\sigma_r = 0.247, \sigma_g = 0.244, \sigma_b = 0.262$. Each channel pixel is normalized by subtracting the mean value in this color channel and then divided by the standard deviation of this color channel.

Table 18. The time costs on conducting SVD over the partially trained vanilla full-rank network to find the initialization model for the hybrid network. The run time results are averaged from 5 independent trials.

Method	Time Cost (in sec.)
ResNet-50 on ImageNet	2.2972 ± 0.0519
WideResNet-50-2 on ImageNet	4.8700 ± 0.0859
VGG-19-BN on CIFAR-10	1.5198 ± 0.0113
ResNet-18 on CIFAR-10	1.3244 ± 0.0201
LSTM on WikeText-2	6.5791 ± 0.0445
Transformer on WMT16	5.4104 ± 0.0532

The ImageNet dataset. For ImageNet, we follow the data augmentation process of (Goyal et al., 2017), *i.e.*, we use scale and aspect ratio data augmentation. The network input image is a 224×224 pixels, randomly cropped from an augmented image or its horizontal flip. The input image is normalized in the same way as we normalize the CIFAR-10 images using the following means and standard deviations: $\mu_r = 0.485, \mu_g = 0.456, \mu_b = 0.406$; $\sigma_r = 0.229, \sigma_g = 0.224, \sigma_b = 0.225$.

I DETAILED HYPER-PARAMETERS USED IN OUR EXPERIMENTS

ResNet-50 and WideResNet-50-2 over the ImageNet dataset. For ResNet-50 and WideResNet-50-2 models, we follow the model training hyper-parameters reported in (Goyal et al., 2017). We train the model using the optimizer SGD with momentum value at 0.9 with batch size at 256. We also conduct ℓ_2 regularization over the model weights instead of the BatchNorm layers with the regularization coefficient 10^{-4}. The entire training process takes 90 epochs. For both of the ResNet-50 and WideResNet-50-2 models, we start from the learning rate at 0.1 and decay the learning rate by a factor of 0.1 at the 30-th, 60-th, and the 80-th epochs. For the vanilla warm-up training, we use warm-up epoch $E_{wu} = 10$. Note that at the 10-th epoch we switch from the vanilla ResNet-50/WideResNet-50-2 models to the hybrid architecture, but we still use the same learning rate, *i.e.*, 0.1 until the 30-th epoch. Additional to the previously proposed work, we adopt the *label smoothing* technique with probability 0.1. The model initialization method follows directly from the implementation of PyTorch example [7].

ResNet-18 and VGG-19-BN over the CIFAR-10 dataset. For ResNet-18 and VGG-19-BN models. We train the model

[7] https://github.com/pytorch/examples/tree/master/imagenet

using the optimizer SGD with momentum with momentum value at 0.9 with batch size at 128. The entire training takes 300 epochs. We also conduct ℓ_2 regularization over the model weights with the regularization coefficient 10^{-4}. For both of the ResNet-18 and VGG-19-BN models, we start from the learning rate at 0.1 and decay the learning rate by a factor of 0.1 at the 150-th, 250-th epochs. For the vanilla warm-up training, we use warm-up epoch $E_{wu} = 80$. Note that at the 80-th epoch we switch from the vanilla ResNet-18/VGG-19-BN models to the hybrid architecture, but we still use the same learning rate, *i.e.*, 0.1 until the 150-th epoch.

LSTM over the WikiText-2 dataset. For the LSTM model, we conduct training using the vanilla SGD optimizer with batch size at 20. We also conduct gradient norm clipping with norm bound at 0.25. The entire training takes 40 epochs. We start from the learning rate at 20 and decay the learning rate by a factor of 0.25 if the validation loss is not decreasing. For the vanilla warm-up training, we use warm-up epoch $E_{wu} = 10$. Note that at the 10-th epoch we switch from the vanilla LSTM model to the hybrid architecture, we also decay the learning rate by a factor of 0.5. We also tie the word embedding and SoftMax weights (Press & Wolf, 2016).

The Transformer over the WMT16 dataset. For the Transformer model, we use the Adam optimizer with initial learning rate at 0.001, $\beta s = (0.9, 0.98), \epsilon = 10^{-8}$ batch size at 256. We also conduct gradient norm clipping with norm bound at 0.25. The entire training takes 400 epochs. For the vanilla warm-up training, we use warm-up epoch $E_{wu} = 10$. We enable label smoothing, weight sharing for the source and target word embedding, and weight sharing between target word embedding and the last dense layer.

J DETAILED INFORMATION ON THE RUNTIME MINI-BENCHMARK

In the experiment section, we discussed that in the reproducibility optimized setting, factorized networks achieve promising runtime speedup over the vanilla networks. However, sometimes users prefer faster runtime to reproducibility where the speed optimized setting is used (with `cudnn.benckmark` enabled and `cudnn.deterministic` disabled). We also study the runtime of the factorized network under the speed optimized setting. The results are shown in Table 19, from which we observe that the speedup of the factorized network is less promising compared to the reproducibility optimized setting especially for the VGG-19-BN network. However, PUFFERFISH ResNet-18 still achieves $1.16\times$ per-epoch speedup. We leave exploring the optimal model training speed of the factorized networks as the future work.

Table 19. The runtime mini-benckmark results of PUFFERFISH and vanilla VGG-19-BN and ResNet-18 networks training on the CIFAR-10 dataset, results averaged over 10 epochs. Experiment running on a single V100 GPU with batch size at 128; Over the optimized cuDNN implementation with `cudnn.benckmark` enabled and `cudnn.deterministic` disabled; Speedup calcuated based on the averaged per-epoch time.

Model Archs.	Epoch Time (sec.)	Speedup	MACs (G)
Vanilla VGG-19	8.27 ± 0.07	–	0.4
PUFFERFISH VGG-19	$\mathbf{8.16} \pm 0.12$	$\mathbf{1.01}\times$	**0.29**
Vanilla ResNet-18	11.15 ± 0.01	–	0.56
PUFFERFISH ResNet-18	$\mathbf{9.61} \pm 0.08$	$\mathbf{1.16}\times$	**0.22**

K TIME COST MEASUREMENT ON AMAZON EC2

We use the `p3.2xlarge` instances for the distributed experiments, the bandwidth of the instance is "Up to 10 Gbps" as stated on the Amazon EC2 website, *i.e.*, `https://aws.amazon.com/ec2/instance-types/p3/`. For some tasks (especially for the ResNet-50 and WideResNet-50-2), we observe that the bandwidth of the `p3.2xlarge` instance decays sharply in the middle of the experiment. The time costs for ResNet-50 trained on the ImageNet dataset under our prototype `allreduce` distributed implementation are collected when there is no bandwidth decay, *e.g.*, under 10 Gbps. For the DDP time cost results, we run the experiments till the per-epoch time costs become stable, then measure the per-epoch time. For ResNet-18 trained on the CIFAR-10 dataset experiments under our prototype `allreduce` distributed implementation, we do not observe significant bandwidth decay for the `p3.2xlarge` instances. All distributed experiments are conducted under the `us-west-2c` availability zone of EC2.

L ADDITIONAL EXPERIMENTAL RESULTS

The ablation study on the accuracy mitigation strategy over CIFAR-10 and ImageNet. The ablation study results are shown in Table 20 for the LSTM trained on WikiText-2 task, Table 21 for ResNet-50 trained on ImageNet task, and Table 22 for VGG-19-BN trained over CIFAR-10. For the vanilla low-rank ResNet-50 trained on ImageNet, we do not deploy the label smoothing and the extra learning rate decay (with a factor 0.1) at the 80-th epoch.

Table 20. The effect of vanilla warm-up training on the low-rank LSTM trained over WikiText-2. Results are averaged across 3 independent trials with different random seeds.

Methods	Low-rank LSTM (wo. vanilla warm-up)	Low-rank LSTM (w. vanilla warm-up)
Train Ppl.	68.04 ± 2.98	$\mathbf{62.2 \pm 0.74}$
Val. Ppl.	97.59 ± 0.69	$\mathbf{93.62 \pm 0.36}$
Test Ppl.	92.04 ± 0.54	$\mathbf{88.72 \pm 0.24}$

Table 21. The effect of vanilla warm-up training and hybrid network architectures of PUFFERFISH of the low-rank ResNet-50 trained over the ImageNet dataset

Model architectures	Test Acc. Top1	Test Acc. Top5
Low-rank ResNet-50	71.03%	90.26%
Hybrid ResNet-50 (wo. vanilla warm-up)	75.85%	92.96%
Hybrid ResNet-50 (w. vanilla warm-up)	$\mathbf{76.43}\%$	$\mathbf{93.10}\%$

Table 22. The effect of vanilla warm-up training and hybrid network architectures of PUFFERFISH of the low rank VGG-19-BN trained over the CIFAR-10 dataset. Results are averaged across 3 independent trials with different random seeds.

Model architectures	Test Loss	Test Accuracy
Low-rank VGG-19-BN	0.355 ± 0.012	$93.34 \pm 0.08\%$
Hybrid VGG-19-BN (wo. vanilla warm-up)	0.407 ± 0.008	$93.53 \pm 0.13\%$
Hybrid VGG-19-BN (w. vanilla warm-up)	0.375 ± 0.019	$\mathbf{93.89} \pm 0.14\%$